Acta Mech 233, 641–663 (2022)
https://doi.org/10.1007/s00707-021-03129-8

ORIGINAL PAPER

Nils Cwiekala · Heinrich Traphöner · Peter Haupt · Till Clausmeyer · A. Erman Tekkaya

Analytical model of the in-plane torsion test

Received: 12 October 2021 / Revised: 3 December 2021 / Accepted: 11 December 2021 / Published online: 24 January 2022

Abstract In research and industry, the in-plane torsion test is applied to investigate the material behaviour at large plastic strains: a sheet is clamped in two concentric circles, the boundaries are twisted against each other applying a torque, and simple shear of the material arises. This deformation is analysed within the scope of finite elasto-plasticity. An additive decomposition of the Almansi strain tensor is derived, valid as an approximation for arbitrary large plastic strains and sufficiently small elastic strains and rotations. Constitutive assumptions are the von Mises yield criterion, an associative flow rule, isotropic hardening, and a physically linear elasticity relation. The incremental formulation of the elasticity relation applies covariant Oldroyd derivatives of the stress and the strain tensors. The assumptions combined with equilibrium conditions lead to evolution equations for the distribution of stresses and accumulated plastic strain. The nonzero circumferential stress must be determined from the equilibrium condition because no deformation is present in tangential direction. As a result, a differential-algebraic-equation (DAE) system is derived, consisting of three ordinary differential equations combined with one algebraic side condition. As an example material, properties of a dual phase steel DP600 are analysed numerically at an accumulated plastic strain of 3.0. Radial normal stresses of 3.1% and tangential normal stresses of 1.0% of the shear stresses are determined. The influence of the additional normal stresses on the determination of the flow curve is 0.024%, which is negligibly small in comparison with other experimental influences and measurement accuracies affecting the experimental flow curve determination.

List of symbols

$\mathbf{A}$	Almansi tensor
$\boldsymbol{A}_\mathrm{e}$	Elastic part of the Almansi Tensor
$\boldsymbol{A}_\mathrm{p}$	Plastic part of the Almansi Tensor
$\mathbf{D}$	Strain rate tensor
$\boldsymbol{E}$	Green tensor
ε_{ik}	Strain components
$\hat{\boldsymbol{E}}_\mathrm{e}$	Elastic part of the Green tensor
$\overline{\varepsilon}_\mathrm{p}$	Accumulated plastic strain
$\boldsymbol{\varepsilon}$	Linearised strain tensor
$\overline{\varepsilon}$	Equivalent strain

N. Cwiekala · H. Traphöner (✉) · T. Clausmeyer · A. E. Tekkaya
Institute of Forming Technology and Lightweight Components, TU Dortmund University, Baroper Str. 303, 44227 Dortmund, Germany
e-mail: heinrich.traphoener@iul.tu-dortmund.de

P. Haupt
Department of Mechanical Engineering, University of Kassel, Mönchebergstr. 7, 34109 Kassel, Germany

η	Shear angle
$\boldsymbol{F}$	Deformation gradient
$\hat{\boldsymbol{F}}_{\mathrm{e}}$	Elastic part of the deformation gradient
$\boldsymbol{F}_{\mathrm{p}}$	Plastic part of the deformation gradient
F	Yield function
G	Shear modulus
$\hat{\boldsymbol{\Gamma}}$	Total strain tensor related to the intermediate configuration
γ	Shear strain
h	Thickness of the specimen
$\boldsymbol{I}$	Unit tensor
$\boldsymbol{L}$	Spatial velocity gradient
λ	Plastic multiplier
M	Applied Moment
$\overset{\Delta}{(\bullet)}$	Oldroyd derivative of a tensorial quantity
(R, Φ, Z) (r, φ, z)	Cylindrical coordinates in the reference and current configuration
$\hat{\boldsymbol{R}}_{\mathrm{e}}$	Elastic rotation tensor
$r_{\mathrm{I}}, r_{\mathrm{O}}$	Inner and outer radius of the specimen
r_{Y}	Yield radius
$\boldsymbol{S}$	Cauchy stress tensor
$\boldsymbol{S}^{\mathrm{dev}}$	Deviatoric part of $\boldsymbol{S}$
$\tilde{\boldsymbol{S}}$	Convected stress tensor
σ_{ik}	Cauchy stresses
τ	Shear stress
$\hat{\boldsymbol{U}}_{\mathrm{e}}$	Elastic right stretch tensor
(X, Y, Z) (x, y, z)	Cartesian coordinates in the reference and current configuration

1 Introduction

The experimental identification of material parameters and functions is one key aspect of every numerical process analysis. More specifically, in elasto-plasticity flow curves and flow rules are applied to represent the inelastic material behaviour. Experiments for a precise determination of flow curves should perform ideal deformations or ideal strain and stress states. Mathematically, these states are exact solutions of the basic equations: they satisfy the equilibrium conditions and the constitutive equations of a certain class of materials. If an ideal deformation can be performed experimentally, it is possible to calculate stresses and strains from forces and displacements. These are the only physical quantities which can be measured.

A large number of tests and specimens have been developed for the characterisation of sheet metals under simple shear. Simple shear tests such as the shear test according to Miyauchi [1] or according to ASTM B 831 [2] show strong edge influences and notch effects. Due to the increasing inhomogeneity of the stress state, many of the conventional shear tensile tests cannot be evaluated until fracture. Increasing the load, the edge influences will dominate such that the state of simple shear is lost [3]. A characterisation of the fracture strain under ideal simple shear conditions is impossible. Different test methods and samples have been developed to improve the state stress until fracture. One approach is to modify the notches that describe the shear area. Peirs et al. [4] and Roth and Mohr [5] examined the stress state for different notches and defined a new sample based on the results. A second approach is to modify the local thickness in the shear area by removing material from the surface (e.g. [6] or [7]). Despite all efforts, an approximately ideal simple shear is only achieved in a small area around the centre of the test area. The calculation of the local stresses in the test area from the measured force is not possible for these specimens.

A deformation which can be put into practice for rather large rotations and moments is the in-plane torsion. The in-plane torsion test is the only test known enabling ideal simple shear deformation experimentally. This test has been first applied by Marciniak [8] for the characterisation of the flow curve and the Bauschinger effect of copper. The determination of flow curves with accumulated plastic strains up to 1.0 as well as the process limits were investigated by Tekkaya et al. [9]. The theoretical description of instability due to wrinkling

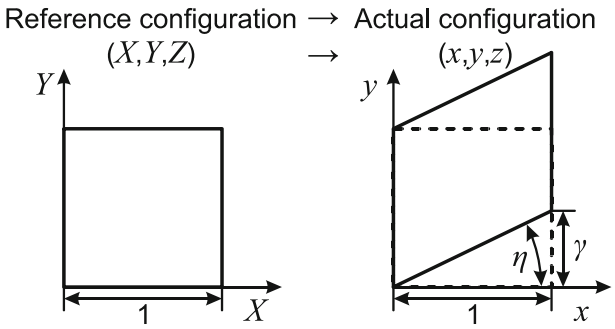

Fig. 1 Simple shear deformation

was described by Bauer [10]. Due to the test evaluation using digital image correlation (DIC) [11] and the development of different samples and test methods, the in-plane torsion test is nowadays used for a variety of applications for the characterisation of sheet metals and components. Wagner et al. [12] also analysed the applicability of the in-plane torsion test in an industrial environment. An extension of Grolleau et al. [13] by the full-field strain measurement enabled the determination of planar anisotropic behaviour. The characterisation of magnesium sheets at elevated temperatures up to 300 °C has been presented by Dardaei Joghan et al. [14]. In combination with bulge tests, the characterisation of transverse hardening was possible [15]. An overview of the applications and the benefits of the experiment was summarised by Traphöner et al. [16].

Although very large equivalent plastic strains up to 3.0 can be achieved in the in-plane torsion test [17], one basic discussion focusses on the stress and strain states: by use of the FEM, Sowerby et al. [18] showed that there are radial and tangential normal stresses and strains for elastic and plastic deformations. Their results indicate that neglecting the additional stresses and strains does not produce a significant error in the evaluation of the test. Bauer [19] confirmed these results experimentally by applying circles to samples and determining the change in their diameter of these circles. He observed small radial strains which he also classifies as negligible. An analytical determination of the deviation, which clearly represents the occurring effects and influences, does not exist.

In the present work, analytical solutions for the in-plane torsion test for small elastic and large plastic deformations are considered to estimate the error by the traditional method of evaluation.

2 Simple shear deformation for large strains

The simple shear deformation is shown in Fig. 1:

It is defined by

$$x = X, \quad y = Y + \gamma X, \quad z = Z, \quad \gamma = \tan(\eta). \tag{1}$$

This deformation transforms a unit square into a rhomboid, the deformation gradient is

$$\boldsymbol{F} = \begin{bmatrix} 1 & 0 & 0 \\ \gamma & 1 & 0 \\ 0 & 0 & 1 \end{bmatrix}. \tag{2}$$

The representation of simple shear is often simplified using the linearised strain tensor:

$$\boldsymbol{\varepsilon} = \frac{1}{2}\begin{bmatrix} 0 & \gamma & 0 \\ \gamma & 0 & 0 \\ 0 & 0 & 0 \end{bmatrix}. \tag{3}$$

However, considering finite, i.e. large deformations, it is easy to see that ideal simple shear deformations, as shown in Fig. 1, give rise to normal strains, too. In fact, finite strain measures like the Green–Lagrange strain tensor $\boldsymbol{E}$ or Almansi strain tensor $\boldsymbol{A}$ contain a normal strain component in addition to the shear strain:

$$\boldsymbol{E} = \frac{1}{2}\left(\boldsymbol{F}^T\boldsymbol{F} - \boldsymbol{1}\right) = \frac{1}{2}\begin{bmatrix} \gamma^2 & \gamma & 0 \\ \gamma & 0 & 0 \\ 0 & 0 & 0 \end{bmatrix}, \quad \boldsymbol{A} = \frac{1}{2}\left(\boldsymbol{1} - \boldsymbol{F}^{T-1}\boldsymbol{F}^{-1}\right) = \frac{1}{2}\begin{bmatrix} -\gamma^2 & \gamma & 0 \\ \gamma & 0 & 0 \\ 0 & 0 & 0 \end{bmatrix}. \tag{4}$$

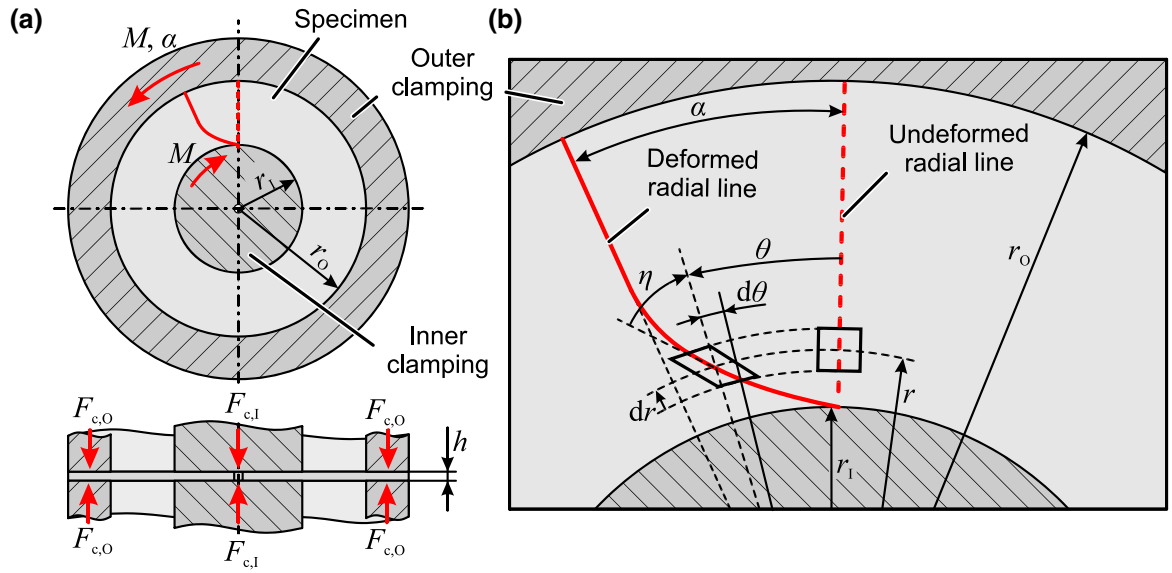

Fig. 2 **a** Principle of the in-plane torsion test and **b** deformation of a radial line

In metal forming processes the deformations usually are rather large and this fact necessitates the application of the exact nonlinear deformation theory. Deviations from the simple state of one shear stress have been discussed, e.g. by Nunes and Moreira [20, 21] for different constitutive models. Furthermore, it was shown by Destrade et al. [22] that the deformation resulting from a simple state of one shear stress does not correspond to the deformation shown in Fig. 1. There is no shear test performing a simple shear deformation combined with a state of only one shear stress. Poynting [23], for example, demonstrated for elastic cylindrical rods that changes of length occur under torsional loads. This so-called Poynting effect results from the additional normal strain components shown in Eq. (4).

3 In-plane torsion test

3.1 Test principle

The principle of the in-plane torsion test is shown in Fig. 2a. A plane round sheet is clamped using fixed supports in concentric circular boundaries of radii r_I and r_O. The outer boundary is rotated by an angle α under the action of an applied torque M in the sheet plane. The annular free area between the boundaries deforms elastically and plastically due to the resulting stresses. As a result of the rotation, all radial material lines deform into the same curve, sketched in Fig. 2b. The geometric boundary conditions of this deformation are straightforward. In the perpendicular direction, we have a free surface. Locally, the in-plane torsion produces a simple shear deformation, however, as its amount depends on the radius r, it is an inhomogeneous deformation.

3.2 Assumptions and evaluation

Classically, the in-plane torsion test is evaluated as follows: The arising shear stress,

$$\tau = \sigma_{r\varphi} = \frac{M}{2\pi h}\frac{1}{r^2}, \tag{5}$$

is calculated from the overall equilibrium condition for the torque M. In this context it is assumed that the sheet thickness h remains constant during the deformation process. The shear strain,

$$\gamma(r) = \tan(\eta(r)) = r\frac{\mathrm{d}\theta(r)}{\mathrm{d}r}, \tag{6}$$

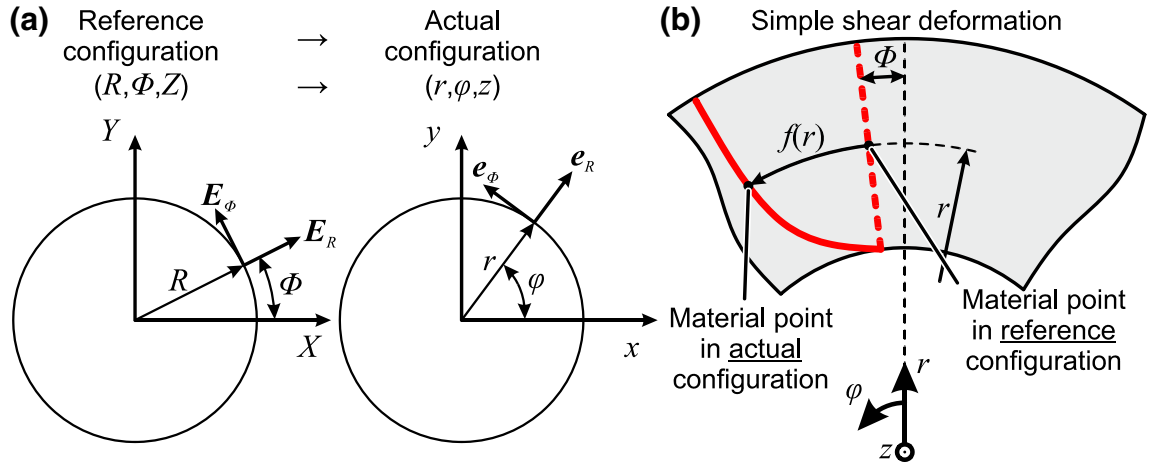

Fig. 3 **a** Deformation defined by a map between actual and reference configuration and **b** ideal simple shear deformation in in-plane torsion tests

follows from the local shear angle η, the slope of the tangent at a point of a deformed material r-line. The experimental determination of the local strains is done by means of DIC. The elements of the DIC to be evaluated are directly coupled to material points. It is assumed that no radial strains occur and the radial positions of the material points do not change. In each step of the evaluation, the initial radius is evaluated.

Conventionally, it is assumed that there is no strain in the z-direction and that no radial and circumferential stresses occur. The equivalent stress and equivalent strain for the given assumptions are

$$\sigma_{\mathrm{Y}} = \sqrt{3} \cdot \tau \sqrt{\frac{2(2r_{\mathrm{n}}+1)}{3(r_{\mathrm{n}}+1)}}, \quad \bar{\varepsilon} = \frac{\gamma}{\sqrt{3}} \sqrt{\frac{3(r_{\mathrm{n}}+1)}{2(2r_{\mathrm{n}}+1)}}, \tag{7}$$

according to the Hill'48 yield criterion and taking the normal anisotropy coefficient r_{n} into account. For isotropic plasticity ($r_{\mathrm{n}} = 1$), Eq. (7) reduces to the v. Mises equivalent stresses and strains:

$$\sigma_{\mathrm{Y}} = \sqrt{3} \cdot \tau \quad \bar{\varepsilon} = \frac{\gamma}{\sqrt{3}}. \tag{8}$$

We will show that these conventional formulas can be applied even for large deformations.

4 Analytical model of the in-plane torsion test

In this Section, the local geometry of the in-plane torsion test is analysed in view of arbitrary large deformations. We exclude radial displacements a priori and assume that the radii of the circumferential material lines remain constant throughout the deformation. In the "Appendix", we supply the equations (though only for the purely elastic behaviour), including also radial displacements. The results show that in this purely elastic case the normal stresses are even reduced (see "Appendix").

The deformation of the in-plane torsion is defined as a map between the reference and the actual configurations. Conveniently, cylindrical coordinate systems are used in both configurations, as shown in Fig. 3a.

The coordinates r and φ represent the position of a material point (R, Φ) in the actual configuration. We have $r_{\mathrm{I}} \leq r \leq r_{\mathrm{O}}$ and $0 \leq \varphi \leq 2\pi$. The axial coordinate z describes the sheet thickness, with $0 \leq z \leq h$. We assume rotational symmetry, i.e. displacements and stresses are independent of the angle φ, they only depend on the radial coordinate r. The locally dependent simple shear deformation is illustrated in Fig. 3b and defined as a map between the reference and the actual coordinate system:

$$r = R, \quad \varphi = \Phi + f(r), \quad z = Z. \tag{9}$$

The experimental set-up is idealised by corresponding boundary conditions: the clamping of the inner boundary is considered by means of a Dirichlet boundary condition $f(r_{\mathrm{I}}) = 0$. The coaxial rigid rotation of the outer boundary corresponds to a condition of combined Dirichlet and Neumann type.

4.1 Basics of finite elasto-plasticity

The kinematic foundation of finite elasto-plasticity is based on the multiplicative decomposition of the deformation gradient into elastic and plastic parts,

$$\boldsymbol{F} = \hat{\boldsymbol{F}}_{\mathrm{e}} \boldsymbol{F}_{\mathrm{p}}. \tag{10}$$

The elastic part $\hat{\boldsymbol{F}}_{\mathrm{e}}$ determines the current state of the Cauchy stress:

$$\boldsymbol{S} = \boldsymbol{g}\left(\hat{\boldsymbol{F}}_{\mathrm{e}}\right), \quad \boldsymbol{g}(\boldsymbol{I}) = \boldsymbol{0}. \tag{11}$$

If no elastic strain is present, the stress vanishes. In this sense, the tensor field $\boldsymbol{F}_{\mathrm{p}}(\boldsymbol{X}, t)$ represents a configuration which is stress free. It is called the intermediate configuration. The intermediate configuration can be illustrated by an imagined process of local unloading.

If the Green strain tensor is formulated in terms of the multiplicative decomposition

$$\boldsymbol{E} = \frac{1}{2}\left(\boldsymbol{F}^T \boldsymbol{F} - \boldsymbol{I}\right) = \frac{1}{2}\left(\boldsymbol{F}_{\mathrm{p}}^T \hat{\boldsymbol{F}}_{\mathrm{e}}^T \boldsymbol{F}_{\mathrm{p}} \hat{\boldsymbol{F}}_{\mathrm{e}} - \boldsymbol{I}\right), \tag{12}$$

a strain tensor $\hat{\boldsymbol{\Gamma}}$ is defined, which is related to the intermediate configuration,

$$\hat{\boldsymbol{\Gamma}} = \boldsymbol{F}_{\mathrm{p}}^{T-1} \boldsymbol{E} \boldsymbol{F}_{\mathrm{p}}^{-1} = \frac{1}{2}\left(\hat{\boldsymbol{F}}_{\mathrm{e}}^T \hat{\boldsymbol{F}}_{\mathrm{e}} - \boldsymbol{I}\right) + \frac{1}{2}\left(\boldsymbol{I} - \boldsymbol{F}_{\mathrm{p}}^{T-1} \boldsymbol{F}_{\mathrm{p}}^{-1}\right). \tag{13}$$

We see that this strain tensor decomposes additively into a purely elastic Green strain tensor

$$\hat{\boldsymbol{E}}_{\mathrm{e}} = \frac{1}{2}\left(\hat{\boldsymbol{F}}_{\mathrm{e}}^T \hat{\boldsymbol{F}}_{\mathrm{e}} - \boldsymbol{I}\right) \tag{14}$$

and a purely plastic Almansi strain tensor

$$\boldsymbol{A}_{\mathrm{p}} = \frac{1}{2}\left(\boldsymbol{I} - \boldsymbol{F}_{\mathrm{p}}^{T-1} \boldsymbol{F}_{\mathrm{p}}^{-1}\right), \tag{15}$$

$$\hat{\boldsymbol{\Gamma}} = \hat{\boldsymbol{E}}_{\mathrm{e}} + \boldsymbol{A}_{\mathrm{p}}. \tag{16}$$

In metal forming, the elastic parts of the strains and rotations are generally negligibly small in comparison with the total strains, which may be arbitrarily large. The transformation of the strain tensor $\hat{\boldsymbol{\Gamma}}$ to the current configuration leads to the total Almansi strain tensor

$$\hat{\boldsymbol{F}}_{\mathrm{e}}^{T-1} \hat{\boldsymbol{\Gamma}} \hat{\boldsymbol{F}}_{\mathrm{e}}^{-1} = \hat{\boldsymbol{F}}_{\mathrm{e}}^{T-1} \boldsymbol{F}_{\mathrm{p}}^{T-1} \boldsymbol{E} \boldsymbol{F}_{\mathrm{p}}^{-1} \hat{\boldsymbol{F}}_{\mathrm{e}}^{-1} = \boldsymbol{F}^{T-1} \boldsymbol{E} \boldsymbol{F}^{-1} = \boldsymbol{A}, \tag{17}$$

and we obtain a decomposition like

$$\boldsymbol{A} = \frac{1}{2}\left(\boldsymbol{I} - \hat{\boldsymbol{F}}_{\mathrm{e}}^{T-1} \hat{\boldsymbol{F}}_{\mathrm{e}}^{-1}\right) + \frac{1}{2}\left(\hat{\boldsymbol{F}}_{\mathrm{e}}^{T-1} \hat{\boldsymbol{F}}_{\mathrm{e}}^{-1} - \hat{\boldsymbol{F}}_{\mathrm{e}}^{T-1}\left(\boldsymbol{F}_{\mathrm{p}}^{T-1} \boldsymbol{F}_{\mathrm{p}}^{-1}\right) \hat{\boldsymbol{F}}_{\mathrm{e}}^{-1}\right). \tag{18}$$

Now, according to the polar decomposition theorem, the elastic deformation gradient decomposes into a rotation and a stretch tensor, $\hat{\boldsymbol{F}}_{\mathrm{e}} = \hat{\boldsymbol{R}}_{\mathrm{e}} \hat{\boldsymbol{U}}_{\mathrm{e}}$, and for small elastic strains we have the approximations $\hat{\boldsymbol{U}}_{\mathrm{e}} \approx \boldsymbol{1}$ or $\hat{\boldsymbol{F}}_{\mathrm{e}} \approx \hat{\boldsymbol{R}}_{\mathrm{e}}$. In this approximate sense, the term $\hat{\boldsymbol{F}}_{\mathrm{e}}^{T-1} \hat{\boldsymbol{F}}_{\mathrm{e}}^{-1}$ equals the unit tensor and in the remaining term $\hat{\boldsymbol{F}}_{\mathrm{e}}^{T-1}\left(\boldsymbol{F}_{\mathrm{p}}^{T-1} \boldsymbol{F}_{\mathrm{p}}^{-1}\right) \hat{\boldsymbol{F}}_{\mathrm{e}}^{-1}$ the elastic rotation is negligible. This leads to the decomposition

$$\boldsymbol{A} = \boldsymbol{A}_{\mathrm{e}} + \boldsymbol{A}_{\mathrm{p}} + O\left(\hat{\boldsymbol{F}}_{\mathrm{e}} - 1\right), \tag{19}$$

which is valid as an asymptotic approximation if the elastic strains and rotations are sufficiently small. In Eq. (19), the Almansi strain tensor $\boldsymbol{A}_{\mathbf{e}}$ characterises the elastic part of the total strain tensor. For small elastic strains and rotations, general equations of elasto-plasticity can be approximately represented in the following form [24]:

$$\text{Decomposition of the strain:} \quad \boldsymbol{A} = \boldsymbol{A}_{\mathrm{e}} + \boldsymbol{A}_{\mathrm{p}}, \tag{20}$$

$$\text{Decomposition of the strain rate:} \quad \overset{\Delta}{\boldsymbol{A}} = \overset{\Delta}{\boldsymbol{A}}_{\mathrm{e}} + \overset{\Delta}{\boldsymbol{A}}_{\mathrm{p}}, \tag{21}$$

$$\text{Isotropic elasticity relation:}\quad \boldsymbol{S} = \boldsymbol{g}(\boldsymbol{A}_\mathrm{e}), \tag{22}$$

$$\text{Yield function :}\quad F\big(\boldsymbol{S}^{\mathrm{dev}}, \sigma_\mathrm{Y}\big) = F\big(\boldsymbol{S}^{\mathrm{dev}}, \sigma_\mathrm{Y}\big(\bar{\varepsilon}_\mathrm{p}\big)\big), \tag{23}$$

$$\text{Flow rule :}\quad \overset{\Delta}{\boldsymbol{A}}_\mathrm{p} = \lambda \frac{\mathrm{d}}{\mathrm{d}\boldsymbol{S}^{\mathrm{dev}}} F\big(\boldsymbol{S}^{\mathrm{dev}}, \sigma_\mathrm{Y}\big) \ \text{ for } F = 0 \,\text{and loading}, \tag{24}$$

$$\text{Accumulated plastic strain :}\quad \dot{\bar{\varepsilon}}_\mathrm{p}(t) = \| \tfrac{2}{3} \overset{\Delta}{\boldsymbol{A}}_\mathrm{p} \| \ \Leftrightarrow \bar{\varepsilon}_\mathrm{p}(t) = \int_{t_0}^{t} \| \tfrac{2}{3} \overset{\Delta}{\boldsymbol{A}}_\mathrm{p}(\bar{t}) \| \mathrm{d}\bar{t}. \tag{25}$$

Here, $\boldsymbol{g}(\bullet)$ is an isotropic function of the elastic strain $\boldsymbol{A}_\mathrm{e}$. Isotropic hardening is incorporated if the yield stress σ_Y depends on the accumulated plastic strain $\bar{\varepsilon}_\mathrm{p}$. Kinematic hardening can be incorporated as well, but this will be omitted here.

The Almansi strain rate is defined as a covariant Oldroyd derivative,

$$\overset{\Delta}{\boldsymbol{A}} = \dot{\boldsymbol{A}} + \boldsymbol{L}^T \boldsymbol{A} + \boldsymbol{A}\boldsymbol{L}, \tag{26}$$

$$\overset{\Delta}{\boldsymbol{A}}_\mathrm{e} = \dot{\boldsymbol{A}}_\mathrm{e} + \boldsymbol{L}^T \boldsymbol{A}_\mathrm{e} + \boldsymbol{A}_\mathrm{e}\boldsymbol{L}, \tag{27}$$

with the spatial velocity gradient $\boldsymbol{L}(r, t) = \dot{\boldsymbol{F}}\, \boldsymbol{F}^{-1}$. The covariant Oldroyd rate of the Almansi strain has an important property: it reduces to the symmetrical part of the velocity gradient, i.e. the classical strain rate tensor:

$$\overset{\Delta}{\boldsymbol{A}} = \boldsymbol{D} = \tfrac{1}{2}\Big(\boldsymbol{L} + \boldsymbol{L}^T\Big). \tag{28}$$

4.2 Formulation of the basic equations

4.2.1 Incremental elasticity relation

In view of small elastic strains, we start with a physically linear isotropic elasticity relation, where no spherical term is needed, since the special deformation under discussion is isochoric:

$$\boldsymbol{S} = 2G\boldsymbol{A} \ (G = \text{shear modulus}). \tag{29}$$

An equivalent incremental elasticity relation can be derived, if Eq. (29) is transformed to a relation between the convected stress, $\tilde{\boldsymbol{S}} = \boldsymbol{F}^T \boldsymbol{S} \boldsymbol{F}$, and the Green strain tensor, $\boldsymbol{E} = \boldsymbol{F}^T \boldsymbol{A} \boldsymbol{F}$,

$$\tilde{\boldsymbol{S}} = 2G\mathbf{E}. \tag{30}$$

This relation can be differentiated with respect to time:

$$\dot{\tilde{\boldsymbol{S}}} = 2G\,\dot{\mathbf{E}}. \tag{31}$$

The inverse transformation then leads to

$$\overset{\Delta}{\boldsymbol{S}} = 2G\,\overset{\Delta}{\boldsymbol{A}}, \tag{32}$$

where we applied the identities $\boldsymbol{F}^{T-1}\, \dot{\tilde{\boldsymbol{S}}}\, \boldsymbol{F}^{-1} = \overset{\Delta}{\boldsymbol{S}}$ and $\boldsymbol{F}^{T-1}\, \dot{\boldsymbol{E}}\, \boldsymbol{F}^{-1} = \overset{\Delta}{\boldsymbol{A}}$.

Within the elasto-plastic range, the incremental elasticity relation reads

$$\overset{\Delta}{\boldsymbol{S}} = 2G\,\overset{\Delta}{\boldsymbol{A}}_\mathrm{e}, \tag{33}$$

and in view of the decomposition from Eq. (21) and the property from Eq. (28), we have

$$\overset{\Delta}{\boldsymbol{S}} = 2G\Big(\boldsymbol{D} - \overset{\Delta}{\boldsymbol{A}}_\mathrm{p}\Big). \tag{34}$$

4.2.2 Deformation gradient, stress and strain tensor

The deformation from Eq. (9),

$$r = R, \quad \varphi = \Phi + f(r), \quad z = Z,$$

implies the deformation gradient

$$\boldsymbol{F} = \begin{bmatrix} 1 & 0 & 0 \\ f'(r) & 1 & 0 \\ 0 & 0 & 1 \end{bmatrix} \left[\boldsymbol{g}_j \otimes \boldsymbol{G}^k\right] = \begin{bmatrix} 1 & 0 & 0 \\ r \cdot f'(r) & 1 & 0 \\ 0 & 0 & 1 \end{bmatrix} \left[\boldsymbol{e}_j \otimes \boldsymbol{E}^k\right]. \tag{35}$$

The brackets behind the matrices symbolise the base systems the matrices are related to. The vectors $\boldsymbol{g}_j$ and $\boldsymbol{G}^k$ represent the tangent and gradient vectors of the actual and the reference configuration, respectively. $\boldsymbol{e}_j$ and $\boldsymbol{E}^k$ form the corresponding unit vectors (representation in physical components). The inverse of $\boldsymbol{F}$ and its transpose read

$$\boldsymbol{F}^{-1} = \begin{bmatrix} 1 & 0 & 0 \\ -r \cdot f'(r) & 1 & 0 \\ 0 & 0 & 1 \end{bmatrix} \left[\boldsymbol{E}_j \otimes \boldsymbol{e}^k\right] \tag{36}$$

and

$$\boldsymbol{F}^T = \begin{bmatrix} 1 & r \cdot f'(r) & 0 \\ 0 & 1 & 0 \\ 0 & 0 & 1 \end{bmatrix} \left[\boldsymbol{E}_j \otimes \boldsymbol{e}^k\right]. \tag{37}$$

The strain tensor, applied in the following analysis, is the Almansi tensor $\boldsymbol{A}$,

$$\boldsymbol{A} = \frac{1}{2}\left(\boldsymbol{I} - \boldsymbol{F}^{T-1}\boldsymbol{F}^{-1}\right) = \frac{1}{2}\begin{bmatrix} -\left(r \cdot f'(r)\right)^2 & r \cdot f'(r) & 0 \\ r \cdot f'(r) & 0 & 0 \\ 0 & 0 & 0 \end{bmatrix} \left[\boldsymbol{e}^j \otimes \boldsymbol{e}^k\right]. \tag{38}$$

This matrix of the Almansi strain is related to the gradient unit vectors in the actual configuration. The same is true for the Cauchy stress,

$$\boldsymbol{S} = \begin{bmatrix} \sigma_{rr} & \sigma_{r\varphi} & 0 \\ \sigma_{\varphi r} & \sigma_{\varphi\varphi} & 0 \\ 0 & 0 & 0 \end{bmatrix} \left[\boldsymbol{e}^j \otimes \boldsymbol{e}^k\right]. \tag{39}$$

The components of $\boldsymbol{S}$ are true stresses.

4.2.3 Equilibrium conditions

The general equilibrium condition for the static case without body forces is given by

$$\operatorname{div}(\boldsymbol{S}) = \begin{bmatrix} \frac{\partial \sigma_{rr}}{\partial r} + \frac{1}{r}\left(\sigma_{rr} - \sigma_{\varphi\varphi}\right) + \frac{1}{r}\frac{\partial \sigma_{r\varphi}}{\partial \varphi} + \frac{\partial \sigma_{rz}}{\partial z} \\ \frac{\partial \sigma_{\varphi r}}{\partial r} + \frac{2}{r}\sigma_{r\varphi} + \frac{1}{r}\frac{\partial \sigma_{\varphi\varphi}}{\partial \varphi} + \frac{\partial \sigma_{\varphi z}}{\partial z} \\ \frac{\partial \sigma_{zr}}{\partial r} + \frac{1}{r}\frac{\partial \sigma_{z\varphi}}{\partial \varphi} + \frac{\partial \sigma_{zz}}{\partial z} + \frac{\sigma_{zr}}{r} \end{bmatrix} = \begin{bmatrix} 0 \\ 0 \\ 0 \end{bmatrix}. \tag{40}$$

For the case of rotational symmetry and plane stress, the equations reduce to

$$\frac{\partial \sigma_{rr}}{\partial r} + \frac{1}{r}(\sigma_{rr} - \sigma_{\varphi\varphi}) = 0, \tag{41}$$

$$\frac{\partial \sigma_{r\varphi}}{\partial r} + \frac{2}{r}\sigma_{r\varphi} = 0. \tag{42}$$

The equilibrium equation in tangential direction (Eq. (42)) is immediately integrated, leading to

$$\sigma_{r\varphi} = \frac{C_1}{r^2}. \tag{43}$$

The constant C_1 is determined based on the boundary condition

$$M = 2\pi \cdot r^2 \cdot h \cdot \sigma_{r\varphi} = 2\pi \cdot h \cdot C_1$$
$$\Leftrightarrow C_1 = \frac{M}{2\pi h}, \tag{44}$$

which is sufficient for determining the shear stress (see Eq. 5):

$$\sigma_{r\varphi} = \frac{M}{2\pi h}\frac{1}{r^2}. \tag{45}$$

4.2.4 Elasticity relations

According to Eq. (29), the stress components are then given as

$$\sigma_{rr} = 2G\varepsilon_{rr} = -G\big(rf'(r)\big)^2, \tag{46}$$

$$\sigma_{r\varphi} = 2G\varepsilon_{r\varphi} = Grf'(r), \tag{47}$$

$$\sigma_{\varphi\varphi} = 0. \tag{48}$$

Now, the function $f(r)$ can be determined for the elastic range: integration of

$$f'(r) = \frac{M}{2\pi Gh}\frac{1}{r^3} \tag{49}$$

leads to

$$f(r) = \frac{M}{2\pi Gh}\frac{1}{r^3} + C_2. \tag{50}$$

The constant C_2 follows from the boundary condition at the inner radius r_I:

$$f(r_\mathrm{I}) = -\frac{M}{4\pi Gh}\frac{1}{r_\mathrm{I}^2} + C_2 = 0 \Rightarrow C_2 = \frac{M}{4\pi Gh}\frac{1}{r_\mathrm{I}^2} \tag{51}$$

resulting in

$$f_\mathrm{el}(r) = \frac{M}{4\pi Gh}\left[\frac{1}{r_\mathrm{I}^2} - \frac{1}{r^2}\right]. \tag{52}$$

According to the elasticity relation, the radial stress distribution follows,

$$\sigma_{rr}(r) = -\frac{1}{G}\left(\frac{M}{2\pi h}\right)^2\frac{1}{r^4}, \tag{53}$$

and the equilibrium in radial direction then leads to

$$\sigma_{\varphi\varphi}(r) = 3G\left(\frac{M}{2\pi h}\right)^2\frac{1}{r^4}. \tag{54}$$

Summarising, we have the following results, valid within the elastic region:

$$f_\mathrm{el}(r) = \frac{M}{4\pi Gh}\left[\frac{1}{r_\mathrm{I}^2} - \frac{1}{r^2}\right], \tag{55}$$

$$\sigma_{rr}(r) = -\frac{1}{G}\left(\frac{M}{2\pi h}\right)^2\frac{1}{r^4}, \tag{56}$$

$$\sigma_{r\varphi}(r) = \frac{M}{2\pi h}\frac{1}{r^2}, \tag{57}$$

$$\sigma_{\varphi\varphi}(r) = 3G\left(\frac{M}{2\pi h}\right)^2\frac{1}{r^4}. \tag{58}$$

The strain distributions are then given as

$$\varepsilon_{rr}(r) = -\frac{1}{2}\left(\frac{M}{2\pi Gh}\right)^2 \frac{1}{r^4}, \tag{59}$$

$$\varepsilon_{r\varphi}(r) = \frac{M}{4\pi Gh}\frac{1}{r^2}, \tag{60}$$

$$\varepsilon_{\varphi\varphi}(r) = \varepsilon_{zz}(r) = 0. \tag{61}$$

Remark: There is a positive circumferential stress, but no corresponding strain. This is no contradiction because the non-vanishing stress $\sigma_{\varphi\varphi}$ is a pure consequence of the equilibrium condition and has nothing to do with any constitutive law. The values of the stresses σ_{rr} and $\sigma_{\varphi\varphi}$ are unequal because σ_{rr} depends on r.

4.2.5 Yield function

The elastic range is limited by means of the yield function and a yield condition. The simplest form of an isotropic yield function is the von Mises function:

$$F\big(\boldsymbol{S}^{\mathrm{dev}}, \sigma_{\mathrm{Y}}\big(\overline{\varepsilon}_{\mathrm{p}}\big)\big) = \tfrac{1}{2}\boldsymbol{S}^{\mathrm{dev}} \cdot \boldsymbol{S}^{\mathrm{dev}} - \tfrac{1}{3}\sigma_{\mathrm{Y}}^2\big(\overline{\varepsilon}_{\mathrm{p}}\big). \tag{62}$$

In case of the in-plane-torsion, this yield function specialises to

$$F\big(\boldsymbol{S}^{\mathrm{dev}}, \sigma_{\mathrm{Y}}\big(\overline{\varepsilon}_{\mathrm{p}}\big)\big) = \tfrac{1}{3}\big(\sigma_{rr}^2 + \sigma_{\varphi\varphi}^2 - \sigma_{rr}\sigma_{\varphi\varphi}\big) + \sigma_{r\varphi}^2 - \tfrac{1}{3}\sigma_{\mathrm{Y}}^2\big(\overline{\varepsilon}_{\mathrm{p}}\big). \tag{63}$$

The corresponding yield condition follows as

$$\tfrac{1}{3}\big(\sigma_{rr}^2 + \sigma_{\varphi\varphi}^2 - \sigma_{rr}\sigma_{\varphi\varphi}\big) + \sigma_{r\varphi}^2 - \tfrac{1}{3}\sigma_{\mathrm{Y}}^2\big(\overline{\varepsilon}_{\mathrm{p}}\big) = 0. \tag{64}$$

To describe isotropic hardening, the yield stress σ_{Y} is a function of the accumulated plastic strain $\overline{\varepsilon}_{\mathrm{p}}$. The time rate of the accumulated plastic strain is defined as the norm of the plastic strain rate,

$$\dot{\overline{\varepsilon}}_{\mathrm{p}}(t) = \sqrt{\tfrac{2}{3}\overset{\Delta}{\boldsymbol{A}}_{\mathrm{p}} \cdot \overset{\Delta}{\boldsymbol{A}}_{\mathrm{p}}} = \lambda\sqrt{\tfrac{2}{3}\frac{\partial F}{\partial \boldsymbol{S}^{\mathrm{dev}}} \cdot \frac{\partial F}{\partial \boldsymbol{S}^{\mathrm{dev}}}} = \lambda\sqrt{\tfrac{2}{3}\boldsymbol{S}^{\mathrm{dev}} \cdot \boldsymbol{S}^{\mathrm{dev}}},$$

$$\dot{\overline{\varepsilon}}_{\mathrm{p}}(t) = \tfrac{2}{3}\lambda\sigma_{\mathrm{Y}}\big(\overline{\varepsilon}_{\mathrm{p}}\big). \tag{65}$$

Inserting the elastic stress distributions just determined, we arrive at an equation which defines the yield radius r_{Y}:

$$\frac{13}{G^2}\left(\frac{M}{2\pi h}\right)^4 \frac{1}{r_{\mathrm{Y}}^8} + 3\left(\frac{M}{2\pi h}\right)^2 \frac{1}{r_{\mathrm{Y}}^4} = \sigma_{\mathrm{Y}}^2\big(\overline{\varepsilon}_{\mathrm{p}}\big)$$

$$\Leftrightarrow r_{\mathrm{Y}} = \sqrt[4]{\frac{1}{\sigma_{\mathrm{Y}}}\left(\frac{M}{2\pi h}\right)^2\left[\sqrt{\frac{9}{4}\frac{1}{\sigma_{\mathrm{Y}}^2} - \frac{13}{G^2}} + \frac{3}{2}\frac{1}{\sigma_{\mathrm{Y}}}\right]}. \tag{66}$$

The yield radius r_{Y} separates the elastic and plastic regions in dependence of the applied moment M:

$$\begin{aligned} r_{\mathrm{Y}} \le r \le r_{\mathrm{O}} &\Rightarrow \text{ Elastic behaviour} \\ r_{\mathrm{I}} \le r \le r_{\mathrm{Y}} &\Rightarrow \text{ Elasto-plastic behaviour.} \end{aligned} \tag{67}$$

In contrast to elasticity relations, which are simply algebraic equations, the plastic behaviour can only be modelled by means of differential equations.

To derive these differential equations, we start from the relevant component representations. The deformation gradient is now assumed to be time dependent, $\boldsymbol{F}(r) \to \boldsymbol{F}(r,t)$:

We specify the velocity gradient,

$$\boldsymbol{L}(r,t) = \dot{\boldsymbol{F}}\,\boldsymbol{F}^{-1} = \begin{bmatrix} 0 & 0 & 0 \\ r\,\dot{f}'(r,t) & 0 & 0 \\ 0 & 0 & 0 \end{bmatrix}\Big[\boldsymbol{e}_j \otimes \boldsymbol{e}^k\Big], \tag{68}$$

and the total strain rate tensor (Oldroyd rate of $\boldsymbol{A}$),

$$\overset{\Delta}{\boldsymbol{A}} = \boldsymbol{D} = \frac{1}{2}\begin{bmatrix} 0 & r\,\dot{f}'(r,t) & 0 \\ r\,\dot{f}'(r,t) & 0 & 0 \\ 0 & 0 & 0 \end{bmatrix}\left[\boldsymbol{e}^j \otimes \boldsymbol{e}^k\right]. \tag{69}$$

The stress rate (Oldroyd rate of $\boldsymbol{S}$) is calculated to be

$$\overset{\Delta}{\boldsymbol{S}} = \dot{\boldsymbol{S}} + \boldsymbol{L}^T\boldsymbol{S} + \boldsymbol{S}\boldsymbol{L} = \begin{bmatrix} \dot{\sigma}_{rr} + 2\sigma_{r\varphi} r\,\dot{f}'(r,t) & \dot{\sigma}_{r\varphi} + \sigma_{\varphi\varphi} r\,\dot{f}'(r,t) & 0 \\ \dot{\sigma}_{r\varphi} + \sigma_{\varphi\varphi} r\,\dot{f}'(r,t) & \dot{\sigma}_{\varphi\varphi} & 0 \\ 0 & 0 & 0 \end{bmatrix}\left[\boldsymbol{e}^j \otimes \boldsymbol{e}^k\right]. \tag{70}$$

To specify the plastic part of the strain rate occurring in the incremental elasticity relation (Eq. (34)),

$$\overset{\Delta}{\boldsymbol{S}} = 2G\left(\boldsymbol{D} - \overset{\Delta}{\boldsymbol{A}}_{\mathrm{p}}\right),$$

we have to observe the particularity of the deformation, a priori assumed by Eq. (9). The assumption implies that the circumferential elastic strain $\varepsilon_{\varphi\varphi\mathrm{e}}$ is identically zero (see Eq. (61)) as well as the total strain rate $\overset{\Delta}{\varepsilon}_{\varphi\varphi}$ (see Eq. (69)). Therefore, the plastic strain rate $\overset{\Delta}{\varepsilon}_{\varphi\varphi\mathrm{p}}$ must vanish as well. The same arguments apply to $\overset{\Delta}{\varepsilon}_{zz\mathrm{p}}$. In this sense, we modify the application of the flow rule (Eq. (24)) and derive the plastic part of the strain rate as

$$\overset{\Delta}{\boldsymbol{A}}_{\mathrm{p}} = \begin{bmatrix} \lambda\left(\frac{2}{3}\sigma_{rr} - \frac{1}{3}\sigma_{\varphi\varphi}\right) & \lambda\sigma_{r\varphi} & 0 \\ \lambda\sigma_{r\varphi} & 0 & 0 \\ 0 & 0 & 0 \end{bmatrix}\left[\boldsymbol{e}^j \otimes \boldsymbol{e}^k\right]. \tag{71}$$

The right-hand side of the incremental elasticity relation (Eq. (34)) then reduces to

$$2G\,\overset{\Delta}{\boldsymbol{A}}_{\mathrm{e}} = 2G\left(\boldsymbol{D} - \overset{\Delta}{\boldsymbol{A}}_{\mathrm{p}}\right) = 2G\begin{bmatrix} -\lambda\left(\frac{2}{3}\sigma_{rr} - \frac{1}{3}\sigma_{\varphi\varphi}\right) & \frac{1}{2}r\,\dot{f}'(r,t) - \lambda\sigma_{r\varphi} & 0 \\ \frac{1}{2}r\,\dot{f}'(r,t) - \lambda\sigma_{r\varphi} & 0 & 0 \\ 0 & 0 & 0 \end{bmatrix}\left[\boldsymbol{e}^j \otimes \boldsymbol{e}^k\right]. \tag{72}$$

4.2.6 Evolution equations

After these preparations, we obtain the evolution equation for the stresses $\sigma_{rr}, \sigma_{r\varphi}, \sigma_{\varphi\varphi}$:

$$\dot{\sigma}_{rr} + 2\sigma_{r\varphi} r\,\dot{f}'(r,t) = -2G\lambda\left(\tfrac{2}{3}\sigma_{rr} - \tfrac{1}{3}\sigma_{\varphi\varphi}\right), \tag{73}$$

$$\dot{\sigma}_{r\varphi} + \sigma_{\varphi\varphi} r\,\dot{f}'(r,t) = 2G\tfrac{1}{2}r\,\dot{f}'(r,t) - 2G\lambda\sigma_{r\varphi}, \tag{74}$$

$$\dot{\sigma}_{\varphi\varphi} = 0. \tag{75}$$

If we introduce the rate of the shear strain $\gamma(t)$,

$$\dot{\gamma}(t) = r\,\dot{f}'(r,t), \tag{76}$$

the evolution equations read

$$\dot{\sigma}_{rr} = -\tfrac{2G}{3}\lambda\left(2\sigma_{rr} - 2\sigma_{\varphi\varphi}\right) - 2\sigma_{r\varphi}\,\dot{\gamma}(t), \tag{77}$$

$$\dot{\sigma}_{r\varphi} = G\,\dot{\gamma}(t) - 2G\lambda\sigma_{r\varphi} - \sigma_{\varphi\varphi}\,\dot{\gamma}(t). \tag{78}$$

The plastic multiplier λ follows from the *consistency condition*, which requires that during plastic deformations the yield condition must be fulfilled: for plastic deformations, the total time derivative of the yield function must vanish equally:

$$\frac{\mathrm{d}}{\mathrm{d}t}F\big(\boldsymbol{S}^{\mathrm{dev}},\sigma_{\mathrm{Y}}\big)=\frac{d}{dt}\big\{\tfrac{1}{3}\big(\sigma_{rr}^2+\sigma_{\varphi\varphi}^2-\sigma_{rr}\sigma_{\varphi\varphi}\big)+\sigma_{r\varphi}^2-\tfrac{1}{3}\sigma_{\mathrm{Y}}^2\big(\bar{\varepsilon}_{\mathrm{p}}\big)\big\}\equiv 0. \tag{79}$$

Differentiating the yield function

$$\begin{aligned}\frac{\mathrm{d}}{\mathrm{d}t}F\big(\boldsymbol{S}^{\mathrm{dev}},\sigma_{\mathrm{Y}}\big)=\tfrac{1}{3}\Big(\big(2\sigma_{rr}-\sigma_{\varphi\varphi}\big)\dot{\sigma}_{rr}(t)+\big(2\sigma_{\varphi\varphi}-\sigma_{rr}\big)\dot{\sigma}_{\varphi\varphi}(t)\Big)\\ +2\sigma_{r\varphi}\dot{\sigma}_{r\varphi}(t)-\tfrac{2}{3}\sigma_{\mathrm{Y}}\big(\bar{\varepsilon}_{\mathrm{p}}\big)\sigma_{\mathrm{Y}}'\big(\bar{\varepsilon}_{\mathrm{p}}\big)\dot{\bar{\varepsilon}}_{\mathrm{p}}(t)\end{aligned} \tag{80}$$

and inserting $\dot{\sigma}_{\varphi\varphi}(t)=0$ as well as the time rate of the accumulated plastic strain $\dot{\bar{\varepsilon}}_{\mathrm{p}}(t)=\frac{2}{3}\lambda\sigma_{\mathrm{Y}}\big(\bar{\varepsilon}_{\mathrm{p}}\big)$, leads to

$$\tfrac{1}{3}\big(2\sigma_{rr}-\sigma_{\varphi\varphi}\big)\dot{\sigma}_{rr}(t)+2\sigma_{r\varphi}\dot{\sigma}_{r\varphi}(t)-\tfrac{4}{9}\lambda\sigma_{\mathrm{Y}}^2\big(\bar{\varepsilon}_{\mathrm{p}}\big)\sigma_{\mathrm{Y}}'\big(\bar{\varepsilon}_{\mathrm{p}}\big)\equiv 0. \tag{81}$$

If we insert the evolution Eqs. (77) and (78) for the stresses and rearrange terms, we arrive at the plastic multiplier

$$\lambda=\frac{\sigma_{r\varphi}\big[G-\frac{2}{3}\big(\sigma_{rr}+\sigma_{\varphi\varphi}\big)\big]}{N}\,\dot{\gamma}(t), \tag{82}$$

with the denominator

$$N=\tfrac{G}{9}\big(2\sigma_{rr}-2\sigma_{\varphi\varphi}\big)^2+2G\sigma_{r\varphi}^2+\tfrac{2}{9}\sigma_{\mathrm{Y}}^2\big(\bar{\varepsilon}_{\mathrm{p}}\big)\sigma_{\mathrm{Y}}'\big(\bar{\varepsilon}_{\mathrm{p}}\big). \tag{83}$$

So far, the evolution equations for the stresses σ_{rr}, $\sigma_{r\varphi}$ are

$$\dot{\sigma}_{rr}=\left\{-\frac{2G}{3}\sigma_{r\varphi}\frac{G-\frac{2}{3}\big(\sigma_{rr}+\sigma_{\varphi\varphi}\big)}{N}\big(2\sigma_{rr}-\sigma_{\varphi\varphi}\big)-2\sigma_{r\varphi}\right\}\dot{\gamma}(t), \tag{84}$$

$$\dot{\sigma}_{r\varphi}=\left\{G-2G\sigma_{r\varphi}^2\frac{G-\frac{2}{3}\big(\sigma_{rr}+\sigma_{\varphi\varphi}\big)}{N}-\sigma_{\varphi\varphi}\right\}\dot{\gamma}(t). \tag{85}$$

Intermediate calculations lead to the final version of the evolution equations:

$$\dot{\sigma}_{rr}=-\frac{2\sigma_{r\varphi}}{N}\{\tfrac{1}{3}\big(2\sigma_{rr}-\sigma_{\varphi\varphi}\big)\big(G^2-G\sigma_{\varphi\varphi}\big)+2G\sigma_{r\varphi}^2+\tfrac{2}{9}\sigma_{\mathrm{Y}}^2\big(\bar{\varepsilon}_{\mathrm{p}}\big)\sigma_{\mathrm{Y}}'\big(\bar{\varepsilon}_{\mathrm{p}}\big)\}\,\dot{\gamma}(t), \tag{86}$$

$$\dot{\sigma}_{r\varphi}=\frac{1}{N}\left\{\big(G-\sigma_{\varphi\varphi}\big)\Big[\tfrac{G}{9}\big(2\sigma_{rr}-\sigma_{\varphi\varphi}\big)^2+\tfrac{2}{9}\sigma_{\mathrm{Y}}^2\big(\bar{\varepsilon}_{\mathrm{p}}\big)\sigma_{\mathrm{Y}}'\big(\bar{\varepsilon}_{\mathrm{p}}\big)\Big]+\tfrac{2}{3}G\sigma_{r\varphi}^2\big(2\sigma_{rr}-\sigma_{\varphi\varphi}\big)\right\}\dot{\gamma}(t), \tag{87}$$

$$\dot{\bar{\varepsilon}}_{\mathrm{p}}(t)=\tfrac{2}{3}\sigma_{r\varphi}\frac{G-\frac{2}{3}\big(\sigma_{rr}+\sigma_{\varphi\varphi}\big)}{N}\sigma_{\mathrm{Y}}\big(\bar{\varepsilon}_{\mathrm{p}}\big)\,\dot{\gamma}(t). \tag{88}$$

4.2.7 Transformation of variables

The evolution equations are invariant with respect to a transformation of time scale, a characteristic property of rate-independent elasto-plasticity. Therefore, the time may be replaced by another loading parameter. In the present situation, it is convenient to choose the shear strain γ as independent variable. This is done by dividing the evolution equations by

$$\dot{\gamma}(t)=\frac{\mathrm{d}\gamma}{\mathrm{d}t} \tag{89}$$

and applying the chain rules

$$\frac{\mathrm{d}\sigma_{rr}(t)}{\mathrm{d}t}\frac{1}{\dot{\gamma}(t)}=\frac{\mathrm{d}\sigma_{rr}(\gamma)}{\mathrm{d}\gamma},\quad \frac{\mathrm{d}\sigma_{r\varphi}(t)}{\mathrm{d}t}\frac{1}{\dot{\gamma}(t)}=\frac{\mathrm{d}\sigma_{r\varphi}(\gamma)}{\mathrm{d}\gamma},\quad \frac{\mathrm{d}\bar{\varepsilon}_{\mathrm{p}}(t)}{\mathrm{d}t}\frac{1}{\dot{\gamma}(t)}=\frac{\mathrm{d}\bar{\varepsilon}_{\mathrm{p}}(\gamma)}{\mathrm{d}\gamma}. \tag{90}$$

The evolution equations now read:

$$\frac{\mathrm{d}\sigma_{rr}(\gamma)}{\mathrm{d}\gamma} = -\frac{2\sigma_{r\varphi}}{N}\left\{\tfrac{1}{3}\left(2\sigma_{rr}-\sigma_{\varphi\varphi}\right)\left(G^2 - G\sigma_{\varphi\varphi}\right) + 2G\sigma_{r\varphi}^2 + \tfrac{2}{9}\sigma_{\mathrm{Y}}^2\left(\overline{\varepsilon}_{\mathrm{p}}\right)\sigma_{\mathrm{Y}}'\left(\overline{\varepsilon}_{\mathrm{p}}\right)\right\}, \tag{91}$$

$$\frac{\mathrm{d}\sigma_{r\varphi}(\gamma)}{\mathrm{d}\gamma} = \frac{1}{N}\left\{\left(G-\sigma_{\varphi\varphi}\right)\left[\tfrac{G}{9}\left(2\sigma_{rr}-\sigma_{\varphi\varphi}\right)^2 + \tfrac{2}{9}\sigma_{\mathrm{Y}}^2\left(\overline{\varepsilon}_{\mathrm{p}}\right)\sigma_{\mathrm{Y}}'\left(\overline{\varepsilon}_{\mathrm{p}}\right)\right] + \tfrac{2}{3}G\sigma_{r\varphi}^2\left(2\sigma_{rr}-\sigma_{\varphi\varphi}\right)\right\}, \tag{92}$$

$$\frac{\mathrm{d}\overline{\varepsilon}_{\mathrm{p}}(\gamma)}{\mathrm{d}\gamma} = \tfrac{2}{3}\sigma_{r\varphi}\frac{G-\frac{2}{3}\left(\sigma_{rr}+\sigma_{\varphi\varphi}\right)}{N}\sigma_{\mathrm{Y}}\left(\overline{\varepsilon}_{\mathrm{p}}\right). \tag{93}$$

A further transformation of variables is apparent because the distribution of the shear stress is known a priori:

$$\sigma_{r\varphi}(r) \equiv \tau(r) = \frac{M}{2\pi h}\frac{1}{r^2}. \tag{94}$$

Therefore, the evolution equations are transformed to τ as the new independent variable.

An inversion of the differential equation for the shear stress τ leads to an equation for the strain γ as a function of τ:

$$\frac{\mathrm{d}\gamma(\tau)}{\mathrm{d}\tau} = \frac{N}{\left(G-\sigma_{\varphi\varphi}\right)\left[\tfrac{G}{9}\left(2\sigma_{rr}-\sigma_{\varphi\varphi}\right)^2 + \tfrac{2}{9}\sigma_{\mathrm{Y}}^2\left(\overline{\varepsilon}_{\mathrm{p}}\right)\sigma_{\mathrm{Y}}'\left(\overline{\varepsilon}_{\mathrm{p}}\right)\right] + \tfrac{2}{3}G\tau^2\left(2\sigma_{rr}-\sigma_{\varphi\varphi}\right)}. \tag{95}$$

If we apply the chain rule in the form

$$\frac{\mathrm{d}(\ldots)}{\mathrm{d}\gamma}\frac{\mathrm{d}\gamma}{\mathrm{d}\tau} = \frac{\mathrm{d}(\ldots)}{\mathrm{d}\tau} \tag{96}$$

to the equations for σ_{rr} and $\overline{\varepsilon}_{\mathrm{p}}$, we arrive at

$$\frac{\mathrm{d}\sigma_{rr}(\tau)}{\mathrm{d}\tau} = -2\tau\frac{\tfrac{1}{3}\left(2\sigma_{rr}-\sigma_{\varphi\varphi}\right)\left(G^2 - G\sigma_{\varphi\varphi}\right) + 2G\tau^2 + \tfrac{2}{9}\sigma_{\mathrm{Y}}^2\left(\overline{\varepsilon}_{\mathrm{p}}\right)\sigma_{\mathrm{Y}}'\left(\overline{\varepsilon}_{\mathrm{p}}\right)}{\left(G-\sigma_{\varphi\varphi}\right)\left[\tfrac{G}{9}\left(2\sigma_{rr}-\sigma_{\varphi\varphi}\right)^2 + \tfrac{2}{9}\sigma_{\mathrm{Y}}^2\left(\overline{\varepsilon}_{\mathrm{p}}\right)\sigma_{\mathrm{Y}}'\left(\overline{\varepsilon}_{\mathrm{p}}\right)\right] + \tfrac{2}{3}G\tau^2\left(2\sigma_{rr}-\sigma_{\varphi\varphi}\right)}, \tag{97}$$

$$\frac{\mathrm{d}\overline{\varepsilon}_{\mathrm{p}}(\tau)}{\mathrm{d}\tau} = \frac{\tfrac{2}{3}\tau\left[G-\tfrac{2}{3}\left(\sigma_{rr}+\sigma_{\varphi\varphi}\right)\right]\sigma_{\mathrm{Y}}\left(\overline{\varepsilon}_{\mathrm{p}}\right)}{\left(G-\sigma_{\varphi\varphi}\right)\left[\tfrac{G}{9}\left(2\sigma_{rr}-\sigma_{\varphi\varphi}\right)^2 + \tfrac{2}{9}\sigma_{\mathrm{Y}}^2\left(\overline{\varepsilon}_{\mathrm{p}}\right)\sigma_{\mathrm{Y}}'\left(\overline{\varepsilon}_{\mathrm{p}}\right)\right] + \tfrac{2}{3}G\tau^2\left(2\sigma_{rr}-\sigma_{\varphi\varphi}\right)}. \tag{98}$$

All these equations include the circumferential stress $\sigma_{\varphi\varphi}$, however, they give no information on how to calculate its evolution. In fact, this is the same situation as in the elastic case, where the circumferential stress could only be determined from the equilibrium condition in r-direction,

$$\sigma_{\varphi\varphi} = r\frac{\mathrm{d}\sigma_{rr}}{\mathrm{d}r} + \sigma_{rr}. \tag{99}$$

Applying the chain rule again, we infer

$$\sigma_{\varphi\varphi} = r\frac{\mathrm{d}\tau}{\mathrm{d}r}\frac{\mathrm{d}\sigma_{rr}}{\mathrm{d}\tau} + \sigma_{rr}, \tag{100}$$

and inserting the equilibrium condition in φ-direction

$$r\frac{\mathrm{d}\tau}{\mathrm{d}r} = -2\tau, \tag{101}$$

we come to

$$\sigma_{\varphi\varphi} = -2\tau\frac{\mathrm{d}\sigma_{rr}(\tau)}{\mathrm{d}\tau} + \sigma_{rr}. \tag{102}$$

Here, we see that the derivative $\frac{\mathrm{d}\sigma_{rr}(\tau)}{\mathrm{d}\tau}$ can be replaced by the evolution equation already present, namely Eq. (97). This leads to the missing equation

$$\sigma_{\varphi\varphi}(\tau) = 4\tau^2\frac{\tfrac{1}{3}\left(2\sigma_{rr}-\sigma_{\varphi\varphi}\right)\left(G^2 - G\sigma_{\varphi\varphi}\right) + 2G\tau^2 + \tfrac{2}{9}\sigma_{\mathrm{Y}}^2\left(\overline{\varepsilon}_{\mathrm{p}}\right)\sigma_{\mathrm{Y}}'\left(\overline{\varepsilon}_{\mathrm{p}}\right)}{\left(G-\sigma_{\varphi\varphi}\right)\left[\tfrac{G}{9}\left(2\sigma_{rr}-\sigma_{\varphi\varphi}\right)^2 + \tfrac{2}{9}\sigma_{\mathrm{Y}}^2\left(\overline{\varepsilon}_{\mathrm{p}}\right)\sigma_{\mathrm{Y}}'\left(\overline{\varepsilon}_{\mathrm{p}}\right)\right] + \tfrac{2}{3}G\tau^2\left(2\sigma_{rr}-\sigma_{\varphi\varphi}\right)} + \sigma_{rr}(\tau), \tag{103}$$

which must be added to the set of evolution equations for γ, σ_{rr} and $\bar{\varepsilon}_\mathrm{p}$ as an algebraic side condition.

To summarise the results, we have a system of differential equations which is completed by an algebraic equation, a *DAE system:*

$$\frac{\mathrm{d}\gamma(\tau)}{\mathrm{d}\tau} = \frac{\frac{G}{9}\left(2\sigma_{rr}-2\sigma_{\varphi\varphi}\right)^2 + 2G\sigma_{r\varphi}^2 + \frac{2}{9}\sigma_\mathrm{Y}^2\left(\bar{\varepsilon}_\mathrm{p}\right)\sigma_\mathrm{Y}'\left(\bar{\varepsilon}_\mathrm{p}\right)}{\left(G-\sigma_{\varphi\varphi}\right)\left[\frac{G}{9}\left(2\sigma_{rr}-\sigma_{\varphi\varphi}\right)^2 + \frac{2}{9}\sigma_\mathrm{Y}^2\left(\bar{\varepsilon}_\mathrm{p}\right)\sigma_\mathrm{Y}'\left(\bar{\varepsilon}_\mathrm{p}\right)\right] + \frac{2}{3}G\tau^2\left(2\sigma_{rr}-\sigma_{\varphi\varphi}\right)}, \tag{104}$$

$$\frac{\mathrm{d}\sigma_{rr}(\tau)}{\mathrm{d}\tau} = -2\tau\frac{\frac{1}{3}\left(2\sigma_{rr}-\sigma_{\varphi\varphi}\right)\left(G^2-G\sigma_{\varphi\varphi}\right) + 2G\tau^2 + \frac{2}{9}\sigma_\mathrm{Y}^2\left(\bar{\varepsilon}_\mathrm{p}\right)\sigma_\mathrm{Y}'\left(\bar{\varepsilon}_\mathrm{p}\right)}{\left(G-\sigma_{\varphi\varphi}\right)\left[\frac{G}{9}\left(2\sigma_{rr}-\sigma_{\varphi\varphi}\right)^2 + \frac{2}{9}\sigma_\mathrm{Y}^2\left(\bar{\varepsilon}_\mathrm{p}\right)\sigma_\mathrm{Y}'\left(\bar{\varepsilon}_\mathrm{p}\right)\right] + \frac{2}{3}G\tau^2\left(2\sigma_{rr}-\sigma_{\varphi\varphi}\right)}, \tag{105}$$

$$\frac{\mathrm{d}\bar{\varepsilon}_\mathrm{p}(\tau)}{\mathrm{d}\tau} = \frac{\frac{2}{3}\tau\left[G-\frac{2}{3}\left(\sigma_{rr}+\sigma_{\varphi\varphi}\right)\right]\sigma_\mathrm{Y}\left(\bar{\varepsilon}_\mathrm{p}\right)}{\left(G-\sigma_{\varphi\varphi}\right)\left[\frac{G}{9}\left(2\sigma_{rr}-\sigma_{\varphi\varphi}\right)^2 + \frac{2}{9}\sigma_\mathrm{Y}^2\left(\bar{\varepsilon}_\mathrm{p}\right)\sigma_\mathrm{Y}'\left(\bar{\varepsilon}_\mathrm{p}\right)\right] + \frac{2}{3}G\tau^2\left(2\sigma_{rr}-\sigma_{\varphi\varphi}\right)}, \tag{106}$$

$$\sigma_{\varphi\varphi}(\tau) = 4\tau^2\frac{\frac{1}{3}\left(2\sigma_{rr}-\sigma_{\varphi\varphi}\right)\left(G^2-G\sigma_{\varphi\varphi}\right) + 2G\tau^2 + \frac{2}{9}\sigma_\mathrm{Y}^2\left(\bar{\varepsilon}_\mathrm{p}\right)\sigma_\mathrm{Y}'\left(\bar{\varepsilon}_\mathrm{p}\right)}{\left(G-\sigma_{\varphi\varphi}\right)\left[\frac{G}{9}\left(2\sigma_{rr}-\sigma_{\varphi\varphi}\right)^2 + \frac{2}{9}\sigma_\mathrm{Y}^2\left(\bar{\varepsilon}_\mathrm{p}\right)\sigma_\mathrm{Y}'\left(\bar{\varepsilon}_\mathrm{p}\right)\right] + \frac{2}{3}G\tau^2\left(2\sigma_{rr}-\sigma_{\varphi\varphi}\right)} + \sigma_{rr}(\tau)\,. \tag{107}$$

The initial conditions are:

$$\gamma(\tau_\mathrm{Y}) = \frac{M}{2\pi G h}\frac{1}{r_\mathrm{Y}^2}, \tag{108}$$

$$\sigma_{rr}(\tau_\mathrm{Y}) = -\frac{1}{G}\left(\frac{M}{2\pi h}\right)^2\frac{1}{r_\mathrm{Y}^4}, \tag{109}$$

$$\bar{\varepsilon}_\mathrm{p}(\tau_\mathrm{Y}) = 0. \tag{110}$$

The system determines the 4 functions

$$\gamma(\tau), \sigma_{rr}(\tau), \sigma_{\varphi\varphi}(\tau), \bar{\varepsilon}_\mathrm{p}(\tau). \tag{111}$$

The DAE equations are solved numerically by applying the *MATLAB* programme. Given a numerical solution of the DAE system in form of interpolation functions, the spatial distributions of these quantities are evaluated based on the known stress distribution $\tau(r)$:

$$\gamma(r) = \gamma(\tau(r)),\ \sigma_{rr}(r) = \sigma_{rr}(\tau(r)),\ \sigma_{\varphi\varphi}(r) = \sigma_{\varphi\varphi}(\tau(r)),\ \bar{\varepsilon}_\mathrm{p}(r) = \bar{\varepsilon}_\mathrm{p}(\tau(r)). \tag{112}$$

Finally, the distribution of the angle of rotation in the plastic range, $\varphi = \Phi + f(r)$, requires a further numerical integration:

$$f_\mathrm{pl}(r) = \int_{r_\mathrm{I}}^{r}\frac{1}{\bar{r}}\cdot\gamma(\bar{r})\mathrm{d}\bar{r}\quad (r_\mathrm{I}\le r\le r_\mathrm{Y}). \tag{113}$$

4.3 Application

For one explicit example, we experimentally determined the flow curve of a dual phase steel DP600 in $h =$ 1 mm sheet thickness with the in-plane torsion test. The specimen dimensions are given in Table 1. Isotropic hardening according to the Swift approximation is assumed:

$$\sigma_\mathrm{Y} = C\left(\varepsilon_\mathrm{a}+\bar{\varepsilon}_\mathrm{p}\right)^n. \tag{114}$$

The constants C, n and ε_a were experimentally identified. Their values and the shear modulus are shown in Table 1. The torsional load M is 936,500 N•mm, which correlates to an accumulated plastic strain $\bar{\varepsilon}_\mathrm{p}$ of 3.0 ($\sigma_\mathrm{Y}(\bar{\varepsilon}_\mathrm{p}=3.0) = 1148$ MPa) at the inner clamping radius r_I according to the assumed hardening equation. The resulting yield radius r_Y is 25.73 mm according to Eq. (66) and the given parameters. Figure 4 shows the experimental yield curve as well as the mathematical extrapolation up to an equivalent plastic strain of 3.0.

Figures 5 and 6 visualise the calculated stresses $\tau = \sigma_{r\varphi}$, σ_{rr}, $\sigma_{\varphi\varphi}$, the shear strain γ, the accumulated plastic strain $\bar{\varepsilon}_\mathrm{p}$, and the angle of rotation $\varphi = \Phi + f(r)$ for the given load as functions of the radial position r. The red line illustrates the yield radius r_Y.

Table 1 Dimensions and material model parameters based on a DP600 material in $h = 1$ mm sheet thickness

Specimen dimensions			Elasticity
h in mm	r_I in mm	r_O in mm	G in GPa
1.0	15.0	30.0	76.5
Plasticity (isotropic hardening – Swift model)			
$\sigma_{Y,0}$ in MPa	C in MPa	ε_a in [–]	n in [–]
390.00	975.37	0.00202	0.148

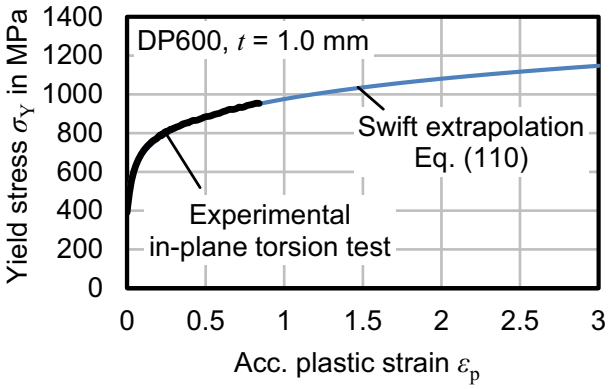

Fig. 4 Experimental yield curve of DP600 from in-plane torsion test and mathematical extrapolation according to Swift

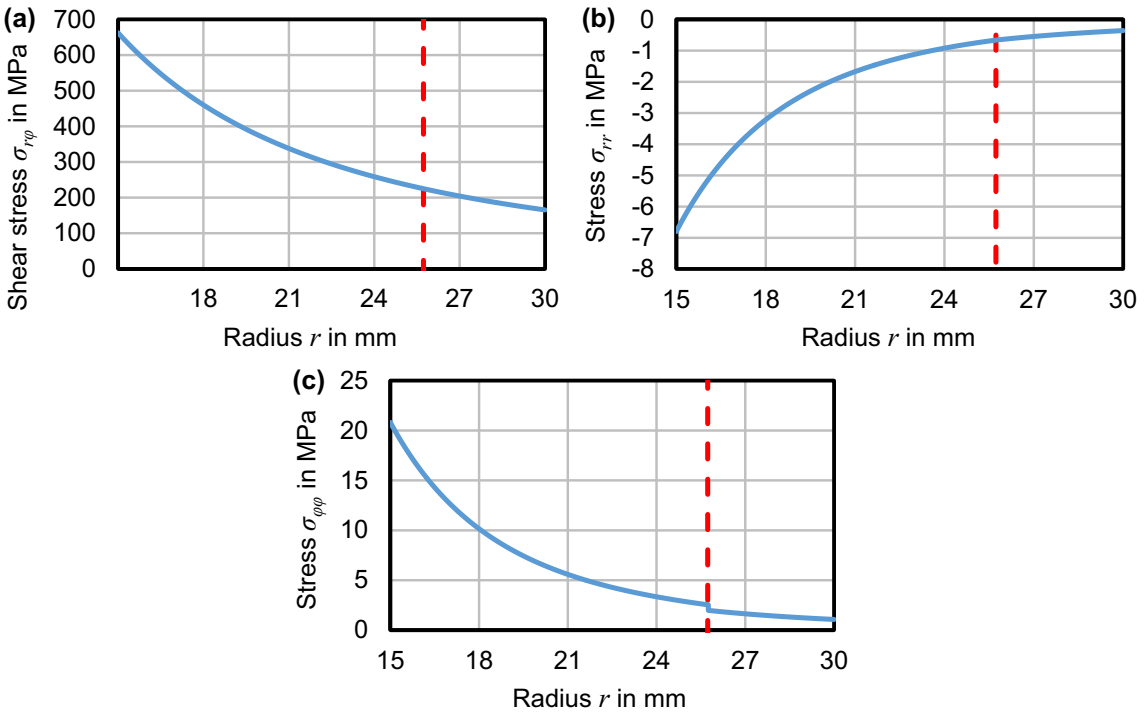

Fig. 5 **a** Shear stress, **b** radial normal stress, and **c** tangential normal stress for the given example

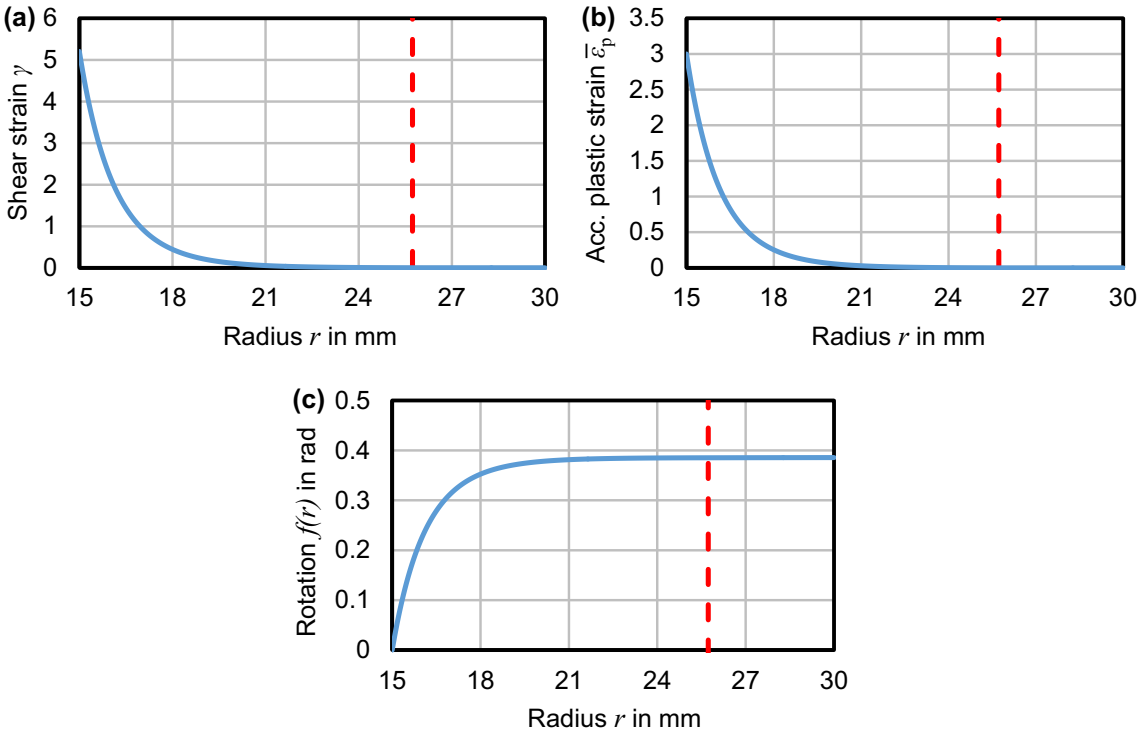

Fig. 6 **a** Shear strain, **b** accumulated plastic strain, and **c** rotation for the given example

The shear stress $\tau = \sigma_{r\varphi}$ is simply the representation of Eq. (5) (Fig. 5a). The normal stresses have a lower order of magnitude as the result of the DAE system. The circumferential stress $\sigma_{\varphi\varphi}$ is discontinuous at $r = r_Y$(see Fig. 5c); this discontinuity is due to the fact that the limit from the left cannot be defined within the initial conditions of the DAE system. A comparison of the shear strain γ (Fig. 6a) with the accumulated plastic strain $\bar{\varepsilon}_p$ (Fig. 6b) shows that Eq. (8) applies quite well as an approximation. From the rotation $\varphi = f(r)$ (Fig. 6c), we see that the elastic region of the disc rotates nearly as a rigid body.

The deformation $\varphi = f(r)$ (rigid body rotation of the φ-lines) may be illustrated by a parameter representation of the form

$$r \mapsto \begin{cases} x = r \cdot \cos(\varphi(r)) \\ y = r \cdot \sin(\varphi(r)) \end{cases}, \quad r_I \le r \le r_O. \tag{115}$$

In this sense, the deformation of the material line with $\Phi = 0$ is depicted in Fig. 7. Figure 7a shows the deformed material line between the inner and outer radius for the example from Figs. 5 and 6 with the moment $M = 936{,}500$ N•mm. The corresponding yield radius is represented by a dashed red line. Figure 7b shows the difference in the deformation with a variation of the applied moment M. We start from a reduced moment of $M = 800{,}000$ N•mm and increase M to $1.4{\cdot}10^6$ N•mm.

5 Discussion

5.1 Influence on the calculation of equivalent stress

In the following, we discuss the influence of the additional normal stresses on the determination of the flow curve based on the in-plane torsion test. For the calculation of the v. Mises equivalent stress according to Eq. (8), $\sigma_Y(\tau) = \sqrt{3}\,\tau$, only the shear stress τ is considered, the additional normal stresses in radial and tangential direction quantified in this work are ignored. In contrast to $\sigma_Y(\tau)$, the exact v. Mises equivalent stress according to Eq. (64) incorporates the normal stress components:

$$\sigma_{Y,\,\text{exact}} = \sqrt{\sigma_{rr}^2 + \sigma_{\varphi\varphi}^2 - \sigma_{rr}\sigma_{\varphi\varphi} + 3\sigma_{r\varphi}^2}. \tag{116}$$

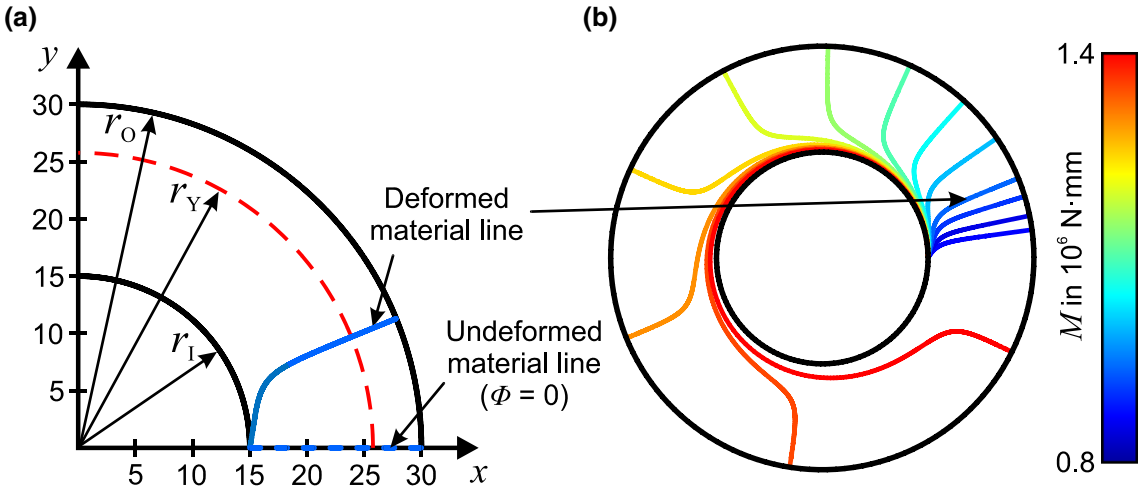

Fig. 7 **a** Deformation of the material line ($\Phi = 0$) for the given example, and **b** deformed material lines for a variation of the moment M

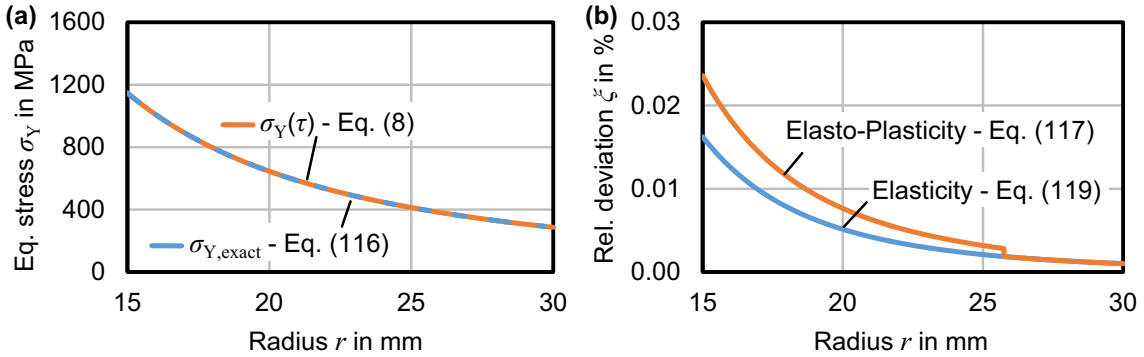

Fig. 8 **a** Equivalent stress values, and **b** relative deviation between equivalent stress calculation with and without taking normal stresses into account

The deviation ξ is defined as

$$\xi = 1 - \frac{\sigma_Y(\tau)}{\sigma_{Y,\,\text{exact}}} = 1 - \frac{\sqrt{3}\,\tau}{\sqrt{\sigma_{rr}^2 + \sigma_{\varphi\varphi}^2 - \sigma_{rr}\sigma_{\varphi\varphi} + 3\tau^2}}. \tag{117}$$

For elastic deformation ($r_Y \le r \le r_O$), the deviation ξ results analytically from the shear stress τ: From Eqs. (56), (57), and (58) there follows

$$\sigma_{rr} = \frac{-\tau^2}{G} \quad \text{and} \quad \sigma_{\varphi\varphi} = 3\frac{\tau^2}{G}. \tag{118}$$

Inserting Eq. (118) in Eq. (117) gives

$$\xi = 1 - \frac{1}{\sqrt{\frac{13}{3}\frac{\tau^2}{G^2} + 1}}. \tag{119}$$

The deviation ξ increases with increasing shear stress τ and decreasing shear modulus G. For the given material parameters from Table 1 ($G = 76.5$ GPa and $\sigma_Y = 1148$ MPa), the maximum deviation is 0.016%. Figure 8b shows the deviation ξ, which decreases with the radial position r.

For elasto-plasticity, the deviation ξ according to Eq. (119) is calculated from the stresses of the numerical solutions. The resulting equivalent v. Mises stresses according to Eqs. (8) and (116) are shown in Fig. 8a. The deviation ξ along the radial distance r is shown in Fig. 8b. The maximum deviation to the classical Eq. (8) is 0.024%, which is negligibly small in comparison with other experimental influences and measurement accuracies influencing the experimental flow curve determination.

5.2 Influence on the calculation of equivalent strain

To interpret the accumulated plastic strain, it can be compared with the plastic part of the shear strain. The plastic shear rate is given by

$$2\overset{\Delta}{\varepsilon}_{r\varphi \mathrm{p}} = \lambda \frac{\partial F}{\partial \sigma_{r\varphi}} = 2\lambda \sigma_{r\varphi} \tag{120}$$

or

$$\dot{\gamma}_{\mathrm{p}}(t) = 2\lambda\tau, \tag{121}$$

and the rate of the accumulated plastic strain is

$$\dot{\overline{\varepsilon}}_{\mathrm{p}}(t) = \tfrac{2}{3}\lambda\sigma_{\mathrm{Y}}. \tag{122}$$

Therefore, we have

$$\frac{\dot{\overline{\varepsilon}}_{\mathrm{p}}(t)}{\dot{\gamma}_{\mathrm{p}}(t)} = \frac{\frac{2}{3}\lambda\sigma_{\mathrm{Y}}}{2\lambda\tau} = \frac{\sigma_{\mathrm{Y}}}{3\tau}, \tag{123}$$

i.e.

$$\dot{\overline{\varepsilon}}_{\mathrm{p,exact}}(t) = \frac{\sigma_{\mathrm{Y}}}{3\tau}\dot{\gamma}_{\mathrm{p}}(t) = \frac{\sqrt{\frac{1}{3}\left(\sigma_{rr}^2 + \sigma_{\varphi\varphi}^2 - \sigma_{rr}\sigma_{\varphi\varphi}\right) + \tau^2}}{\sqrt{3}\tau}\dot{\gamma}_{\mathrm{p}}(t). \tag{124}$$

If no normal stresses are present, this reduces to

$$\dot{\overline{\varepsilon}}_{\mathrm{p}}(t) = \frac{1}{\sqrt{3}}\dot{\gamma}_{\mathrm{p}}(t). \tag{125}$$

Integration with respect to time leads to the equivalent plastic strain of the classical theory, mentioned in Eq. (8):

$$\overline{\varepsilon}_{\mathrm{p}} = \frac{1}{\sqrt{3}}\gamma_{\mathrm{p}}. \tag{126}$$

Following different approaches, Eq. (126) has been confirmed by multiple authors, e.g. Tekkaya [25].

For the given material parameters from Table 1, the resulting accumulated plastic strain according to Eqs. (124) and (126) is shown in Fig. 9a. The deviation ξ between the accumulated plastic strains from Eqs. (126) and (124) is defined as

$$\xi = 1 - \frac{\overline{\varepsilon}_{\mathrm{p}}(\gamma)}{\overline{\varepsilon}_{\mathrm{p,\ exact}}}. \tag{127}$$

The deviation ξ along the radial distance r is shown in Fig. 9. The maximum deviation to the classical Eq. (126) is 0.024%, which is negligibly small in comparison with, e.g., measurement deviations caused by DIC systems.

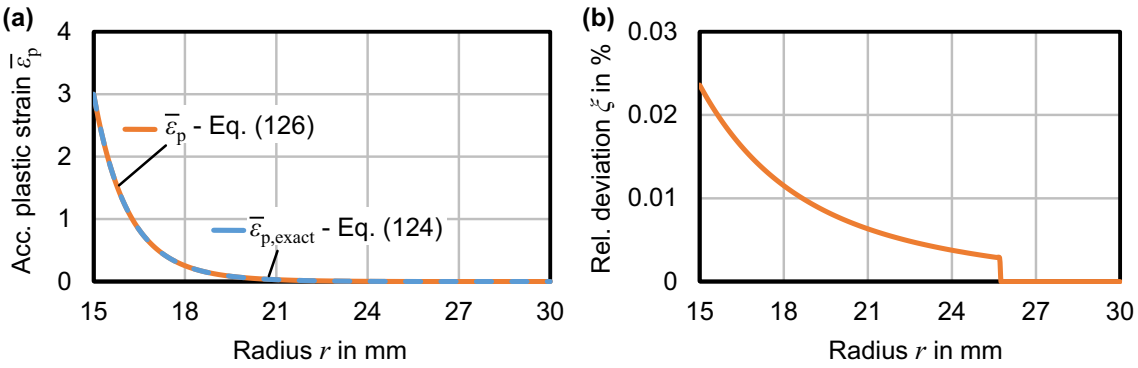

Fig. 9 **a** Accumulated plastic strain values, and **b** relative deviation between accumulated strain calculation with and without taking normal stresses into account

6 Conclusions

Essentially, the in-plane torsion test can be represented as a space-dependent simple shear deformation. A precise investigation within the geometric nonlinear finite strain theory shows normal stress effects. The magnitude of the radial and circumferential stresses depends on the load and the overall angle of rotation and is less than about three per cent of the maximal shear stress. Their influence on the calculation of the equivalent stress and strain values is negligibly small. Hence, the traditional definition of these quantities can be used even for rather large deformations.

A final remark should be added: the radial stresses and strains depend on the radial coordinate. This fact could motivate the conjecture that a radial displacement field might exist, too. Indeed, experimental observations made by Bauer [19] and confirmed by the authors suggest that there are radial displacements in an exceedingly small order of magnitude. These displacements are ignored in our definition of the in-plane torsion as an ideal deformation. Generally, an incorporation of radial displacements leads to a nonlinear boundary value problem in view of the geometric boundary conditions. Assuming pure elasticity, the formulation is straightforward, and a numerical solution is shown in "Appendix". How to obtain a corresponding set of ordinary differential equations in case of elasto-plasticity seems to be an open question.

Acknowledgements The authors acknowledge funding from the German Research Foundation (DFG) for project 327544970.

Funding Open Access funding enabled and organized by Projekt DEAL. Funding was provided by Deutsche Forschungsgemeinschaft (Grant No. 327544970).

Appendix: Elastic solution with radial displacements

For in-plane shear with superimposed radial displacements, the deformation reads

$$r = R + g(r), \quad \varphi = \Phi + f(r), \quad z = Z, \tag{128}$$

and is sketched in Fig. 10.

The physical components of the deformation gradient are calculated as

$$\boldsymbol{F} = \begin{bmatrix} 1 + g'(r) & 0 & 0 \\ r \cdot f'(r) & \frac{r}{R} & 0 \\ 0 & 0 & 1 \end{bmatrix} \left[\boldsymbol{e}_j \otimes \boldsymbol{E}^k \right], \tag{129}$$

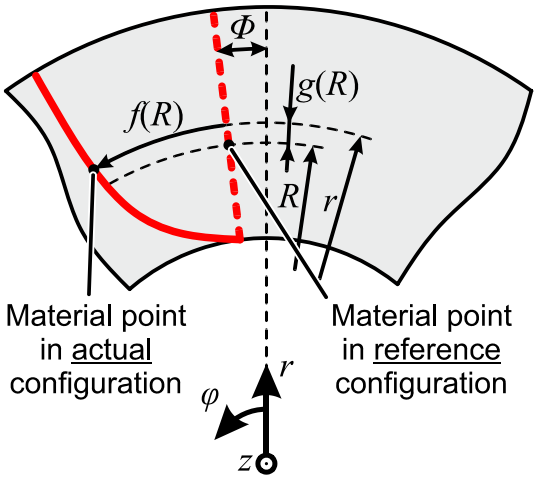

Fig. 10 In-plane torsion deformation with radial displacements

and the Almansi tensor $\boldsymbol{A}$ reads

$$\boldsymbol{A} = \frac{1}{2}\begin{bmatrix} 1 - \frac{\left(R\,f'(R)\right)^2+1}{\left(g'(R)+1\right)^2} & \frac{R^2\,f'(R)}{r(g'(R)+1)} & 0 \\ \frac{R^2\,f'(R)}{r(g'(R)+1)} & 1-\frac{R^2}{r^2} & 0 \\ 0 & 0 & 0 \end{bmatrix}. \tag{130}$$

Employing the elasticity relation from Eq. (29),

$$\boldsymbol{S} = 2\,G\,\boldsymbol{A},$$

results in the following non-vanishing components of the Cauchy stress tensor:

$$\sigma_{r\varphi} = \tau_{r\varphi} = G\,\frac{R^2\,f'(R)}{r(g'(R)+1)}, \tag{131}$$

$$\sigma_{rr} = G\left(1 - \frac{\left(R\,f'(R)\right)^2+1}{\left(g'(R)+1\right)^2}\right), \tag{132}$$

$$\sigma_{\varphi\varphi} = G\left(1-\frac{R^2}{r^2}\right). \tag{133}$$

We do not have any dependencies on the angle or the sheet thickness and, consequently, the equilibrium conditions (Eq. 40) reduces to

$$\frac{\partial\sigma_{rr}}{\partial r} + \frac{1}{r}(\sigma_{rr} - \sigma_{\varphi\varphi}) = 0 \tag{134}$$

$$\frac{\partial\sigma_{r\varphi}}{\partial r} + \frac{2}{r}\sigma_{r\varphi} = 0, \tag{135}$$

as shown for the ideal simple shear deformation. From Eq. (135), we find

$$f'(R) = \frac{M}{2\pi G t}\,\frac{1}{R^2}\,\frac{g'(R)+1}{g(R)+R}, \tag{136}$$

where we followed the same steps as in Eqs. (43) to (45) and made use of Eq. (128). Using Eqs. (131) and (136) as well as the chain rule $\frac{\partial(\bullet)}{\partial r} = \frac{\partial(\bullet)}{\partial R}\left(\frac{\partial r}{\partial R}\right)^{-1}$ in Eq. (134), we derived a second-order differential equation for the radial displacements $g(R)$:

$$g''(R) = \frac{1}{2}\left[-\left(\frac{M}{2\pi G t}\right)^2\left(\frac{\left(g'(R)+1\right)^4}{R^2(g(R)+R)^3} + \frac{2\left(g'(R)+1\right)^3}{R^3(g(R)+R)^2}\right) - \frac{R^2\left(g'(R)+1\right)^4}{(g(R)+R)^3} + \frac{\left(g'(R)+1\right)^2}{(g(R)+R)}\right]. \tag{137}$$

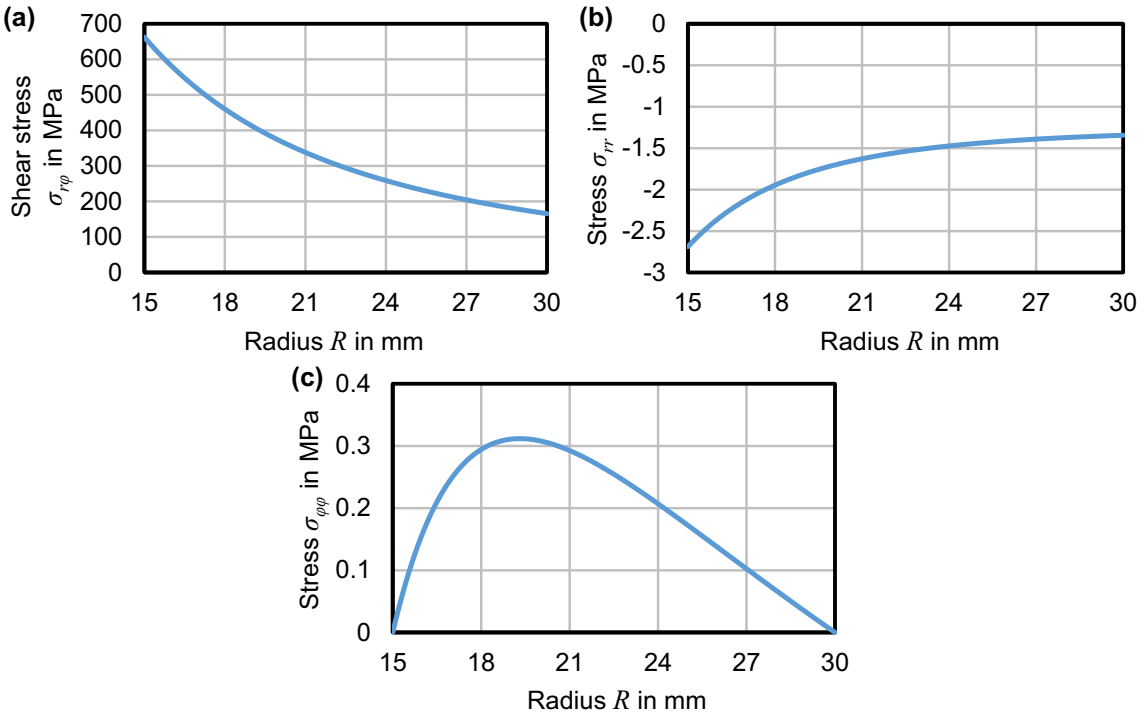

Fig. 11 **a** Shear stress, **b** radial normal stress, and **c** tangential normal stress for the given example

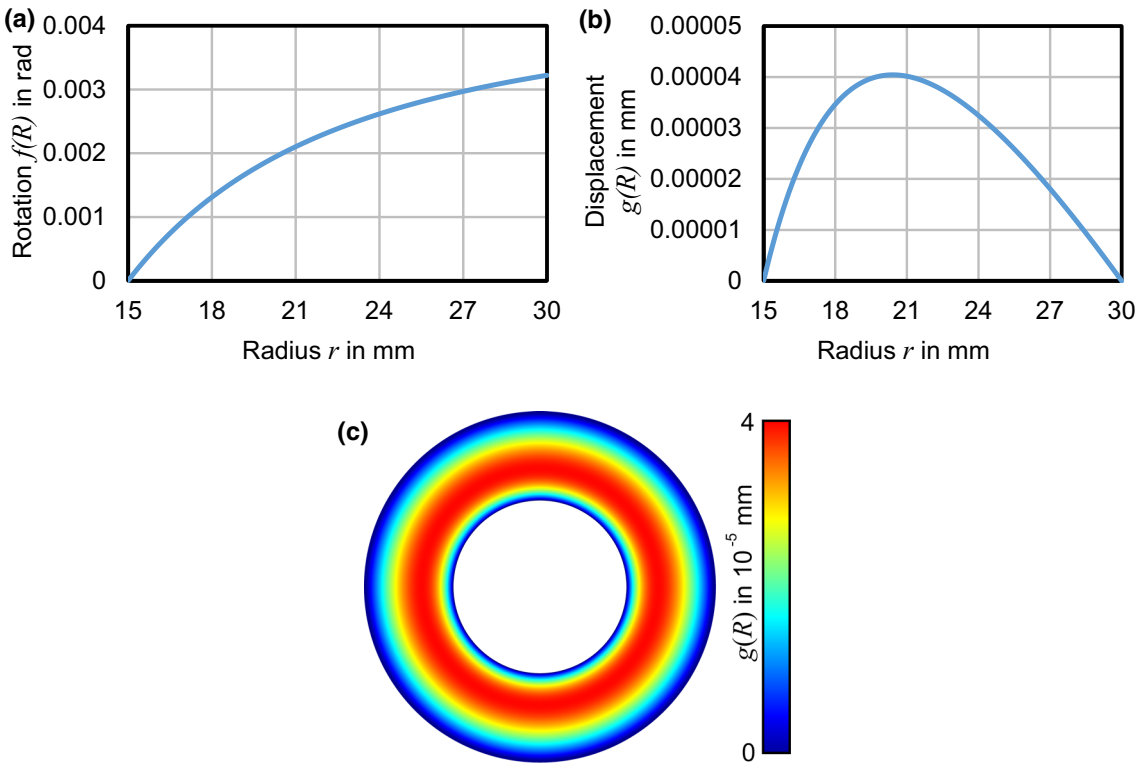

Fig. 12 **a** Tangential rotation, **b** radial displacement, and **c** full-field view of radial displacements for the given example

Equation (137) can be solved numerically employing the boundary conditions

$$g(r_I) = g(r_O) = 0. \tag{138}$$

Figure 11 shows the non-vanishing stress components along the initial radial position R for the elastic material properties and loading used in Sect. 4.3. The moment M is 936,500 N•mm. While the shear stress $\sigma_{r\varphi}$ is similar to the results of Sect. 4.3 for the in-plane torsion test without radial displacements, we find that the radial displacements lead to lower principal stresses in radial and tangential direction. Hence, the resulting deviation in the calculation of equivalent stresses is also lower than for the solution without taking radial displacements into account.

Figure 12a, b shows the tangential and radial displacements along the initial radius R. Figure 12c shows a coloured full-field view of the radial displacements in the annular area of the specimen. The radial displacements have positive values along the entire radius. Hence, the material points move in the direction of the outer radius r_O. The displacement at inner and outer clamping is 0, resulting from the boundary conditions. This extension results in compressive radial normal stresses as shown in Fig. 11b.

No solution has been found for the in-plane torsion with radial displacements and elasto-plastic material behaviour. It might be assumed that a similar effect of lower normal stresses in comparison with the deformation without radial displacements will occur. Lower normal stresses would lead to even reduced deviations in the calculation of equivalent stresses. This hypothesis may be confirmed in future works.

References

1. Miyauchi, K.: A proposal for a planar simple shear test in sheet metals. Sci. Pap. Inst. Phys. Chem. Res. **78**(3), 27–40 (1984)
2. ASTM B 831: Standard test method for shear testing of thin aluminum alloy products (B 831) (2005)
3. Bouvier, S., Gardey, B., Haddadi, H., Teodosiu, C.: Characterization of the strain-induced plastic anisotropy of rolled sheets by using sequences of simple shear and uniaxial tensile tests. J. Mater. Process. Technol. **174**(1–3), 115–126 (2006). https://doi.org/10.1016/j.jmatprotec.2005.04.086
4. Peirs, J., Verleysen, P., Degrieck, J.: Novel technique for static and dynamic shear testing of Ti6Al4V sheet. Exp. Mech. **52**(7), 729–741 (2012). https://doi.org/10.1007/s11340-011-9541-9
5. Roth, C.C., Mohr, D.: Determining the strain to fracture for simple shear for a wide range of sheet metals. Int. J. Mech. Sci. **149**(1), 224–240 (2018). https://doi.org/10.1016/j.ijmecsci.2018.10.007
6. G'Sell, C., Boni, S., Shrivastava, S.: Application of the plane simple shear test for determination of the plastic behaviour of solid polymers at large strains. J. Mater. Sci. **18**(3), 903–918 (1983). https://doi.org/10.1007/BF00745590
7. Bao, Y., Wierzbicki, T.: On fracture locus in the equivalent strain and stress triaxiality space. Int. J. Mech. Sci. **46**(1), 81–98 (2004). https://doi.org/10.1016/j.ijmecsci.2004.02.006
8. Marciniak, Z.: Influence of the sign change of the load on the strain hardening curve of a copper test piece subject to torsion. Arch. Mech. Stosowanej **13**(1), 743–752 (1961)
9. Tekkaya, A.E., Pöhlandt, K., Lange, K.: Determining stress–strain curves of sheet metal in the plane torsion test. CIRP Ann. Manuf. Technol. **31**(1), 171–174 (1982)
10. Bauer, M.: Faltenbildung beim ebenen Torsionsversuch. Ingenieur-Archiv **57**(1), 39–50 (1987). https://doi.org/10.1007/BF00536810
11. Yin, Q., Brosius, A., Tekkaya, A.E.: Modified plane torsion tests for sheet metal characterization. In: Proceedings of the ICTP 2011, Aachen, Germany, pp. 696–701 (2011)
12. Wagner, L., Gross, T., Gruber, P.G., Grillenberger, M., Schagerl, M.: Application of the in-plane torsion test in an industrial environment: Recent advances and remaining challenges. Proceedings of the Forming Technology Forum 2019, Herrsching am Ammersee, Germany (2019)
13. Grolleau, V., Roth, C.C., Mohr, D.: Characterizing plasticity and fracture of sheet metal through a novel in-plane torsion experiment. In: Proceedings of the IDDRG 2019, Enschede, Netherlands (2019)
14. Dardaei Joghan, H., Hahn, M., Traphöner, H., Tekkaya, A.E.: Influence of the preheating strategy on the deep drawing of extruded magnesium alloy ME20 sheets. IOP Conf. Ser. Mater. Sci. Eng. (2019). https://doi.org/10.1088/1757-899x/651/1/012067
15. Gutknecht, F., Gerstein, G., Traphöner, H., Clausmeyer, T., Nürnberger, F.: Experimental setup to characterize flow-induced anisotropy of sheet metals. IOP Conf. Ser. Mater. Sci. Eng. (2018). https://doi.org/10.1088/1757-899X/418/1/012085
16. Traphöner, H., Clausmeyer, T., Tekkaya, A.E.: Material characterization for plane and curved sheets using the in-plane torsion test—an overview. J. Mater. Process. Technol. **257**, 278–287 (2018). https://doi.org/10.1016/j.jmatprotec.2018.02.030
17. Traphöner, H., Clausmeyer, T., Tekkaya, A.E.: Methods for measuring large shear strains in in-plane torsion tests. J. Mater. Process. Technol. (2019). 10.1016/j. jmatprotec.2019.116516
18. Sowerby, R., Tomita, Y., Duncan, J.L.: In-plane torsion testing of sheet metal. J. Mech. Eng. Sci. **19**(5), 213–220 (1977). https://doi.org/10.1243/JMES_JOUR_1977_019_045_02
19. Bauer, M.: Ermittlung der Fließkurven von Feinblechen im ebenen Torsionsversuch. Dr. -Ing. -Dissertation, Universität Stuttgart. https://doi.org/10.1007/978-3-642-83780-7 (1989)
20. Nunes, L., Moreira, D.C.: Simple shear under large deformation: experimental and theoretical analyses. Eur. J. Mech. A. Solids **42**, 315–322 (2013). https://doi.org/10.1016/j.euromechsol.2013.07.002

21. Moreira, D.C., Nunes, L.: Comparison of simple and pure shear for an incompressible isotropic hyperelastic material under large deformation. Polym. Testing **32**(2), 240–248 (2013). https://doi.org/10.1016/j.polymertesting.2012.11.005
22. Destrade, M., Murphy, J.G., Saccomandi, G.: Simple shear is not so simple. Int. J. Non-Linear Mech. **47**(2), 210–214 (2012). https://doi.org/10.1016/j.ijnonlinmec.2011.05.008
23. Poynting, J.H.: On pressure perpendicular to the shear planes in finite pure shears, and on the lengthening of loaded wires when twisted. Proc. R. Soc. Lond. A **82**(557), 546–559 (1909)
24. Haupt, P.: Continuum Mechanics and Theory of Materials. Springer, Berlin (2000)
25. Tekkaya, A.E.: Equivalent strain and stress history in torsion tests. Steel Res. **65**(2), 65–70 (1994). https://doi.org/10.1002/srin.199400928